Leading proton production in deep inelastic scattering at HERA

ZEUS Collaboration

Draft, Version 6.07 post-reading version

30/6/2008

Abstract

The semi-inclusive reaction $e^+p \to e^+Xp$, with a final-state proton carrying a large fraction of the incoming proton energy, $x_L > 0.32$, and transverse momentum squared $p_T^2 < 0.5$ GeV^2, was studied with the ZEUS detector at HERA for exchanged photon virtualities $Q^2 > 3$ GeV^2 and mass of the photon-proton system $45 < W < 225$ GeV, using an integrated luminosity of 12.8 pb^{-1}. Leading protons were detected with the ZEUS leading proton spectrometer. The leading-proton production cross section and rates are presented as a function of x_L, p_T^2, Q^2 and the Bjorken scaling variable, x.

1 Introduction

The presence in the final state of leading particles, which have the same identity as the interacting beams, and carry a large fraction of the beam momentum, is typical of hadron-hadron interactions. The spectrum of leading particles approximately scales with the center-of-mass energy, a property known as limiting fragmentation [1]. The properties of the accompanying final state are also universal when studied as a function of the center-of-mass energy available after excluding the leading particles [2, 3].

Events with a final-state proton carrying a large fraction of the available energy, x_L, but a small transverse momentum, p_T, have been studied in detail in high-energy hadron-proton collisions [4–6]. More recently, the HERA-collider experiments reported measurements of the production of leading protons in ep collisions [7, 8]. Several mechanisms have been suggested to explain the production of leading protons. None of them are, as yet, amenable to calculations based on perturbative quantum chromodynamics (pQCD). This is, in part, a consequence of the small values of p_T of the leading proton which necessitates a non-perturbative approach. Some models [9–13] are based on the Regge formalism, with leading-proton production occurring through t-channel exchanges, both isoscalar and isovector, notably of the Pomeron, Reggeons and pions. These exchanges mediate the interaction between the proton and the hadronic fluctuations of the virtual photon. Other models retain quarks and gluons as fundamental entities, but add non-perturbative elements, such as soft-color interactions (SCI) [14]. Alternatively, the concept of fracture functions offers a QCD framework to describe the leading baryon spectra [15]. Fracture functions are a convolution of parton densities in a hadron under the condition that it has fragmented into a specific hadronic final state.

This paper presents measurements of leading-proton production in e^+p collisions, $e^+p \rightarrow e^+Xp$, with a four-fold increase of statistics compared to an earlier measurement [7]. High-energy protons with low transverse momentum carrying at least a fraction x_L=0.32 of the incoming-proton momentum were measured in the ZEUS leading proton spectrometer (LPS) [16]. The cross sections are presented as a function of the proton variables x_L and p_T^2. The dependence on the Bjorken variable x and on the photon virtuality Q^2 was also studied and compared to that of the inclusive deep inelastic (DIS) reaction $e^+p \rightarrow e^+X$. The measurements cover the kinematic range $Q^2 > 3$ GeV^2 and $45 < W < 225$ GeV, where W is the total mass of the photon-proton system. The data for $x_L > 0.93$ were used in an earlier study [17] to extract the diffractive structure function of the proton.

The leading-proton structure function, $F_2^{\rm LP}$, defined in Section 3, which can be identified with a fracture function, is also presented. The latter parametrizes the spectra of leading particles through parton distribution functions in the proton with an associated leading proton. This approach can be incorporated in Monte Carlo (MC) programs simulating hadronic final states in pp interactions at the LHC [18] and extended cosmic rays showers [19, 20].

2 Experimental set-up

The measurements were performed with data collected in 1997 at the ep collider HERA using the ZEUS detector, when HERA operated with a proton beam energy $E_p = 820$ GeV and a positron beam energy $E_e = 27.5$ GeV.

A detailed description of the ZEUS detector can be found elsewhere [21]. A brief outline of the components which are most relevant for this analysis is given below.

Charged particles were tracked in the central tracking detector (CTD) [22], which operated in a magnetic field of 1.43 T provided by a thin superconducting coil. The CTD consisted of 72 cylindrical drift chamber layers, organized in 9 superlayers covering the polar angle[1] region $15^\circ < \theta < 164^\circ$. The transverse-momentum resolution for full-length tracks was $\sigma(p_T)/p_T = 0.0058 p_T \oplus 0.0065 \oplus 0.0014/p_T$, with p_T in GeV.

The high-resolution uranium–scintillator calorimeter (CAL) [23] consisted of three parts: the forward (FCAL), the barrel (BCAL) and the rear (RCAL) calorimeters. Each part was subdivided transversely into towers and longitudinally into one electromagnetic section (EMC) and either one (in RCAL) or two (in BCAL and FCAL) hadronic sections (HAC). The smallest subdivision of the calorimeter is called a cell. The CAL energy resolutions, as measured under test-beam conditions, were $\sigma(E)/E = 0.18/\sqrt{E}$ for electrons and $\sigma(E)/E = 0.35/\sqrt{E}$ for hadrons (E in GeV).

The position of the scattered positron was determined by combining information from the CAL, the small-angle rear tracking detector [24] and the hadron-electron separator [25].

The LPS [16] was used during the HERA I data taking period (1994-2000) to detect positively charged particles scattered at very small angles and carrying a large fraction of the longitudinal momentum of the incoming proton. It consisted of 54 planes of silicon microstrip detectors grouped into six stations, S1 to S6, and located along the outgoing proton beam line between $Z = 20$ m and $Z = 90$ m.

The stations S1, S2, S3 and S4, S5, S6 can be considered as two independent spectrometers, called s123 and s456, respectively, due to their different phase-space coverage, in particular in azimuth. During data taking, the stations were inserted very close to the proton beam (typically a few mm). Charged particles inside the beampipe were deflected

[1] The ZEUS coordinate system is a right-handed Cartesian system, with the Z axis pointing in the proton beam direction, referred to as the "forward direction", and the X axis pointing left towards the center of HERA. The coordinate origin is at the nominal interaction point.

by the magnetic field of the proton-beamline magnets and measured in the LPS with a resolution better than 1% on the longitudinal momentum and of 5 MeV on the transverse momentum. The beam transverse momentum spread at the interaction point was ≈ 40 MeV in the horizontal plane and ≈ 90 MeV in the vertical plane and dominated the transverse-momentum resolution.

A forward neutron calorimeter (FNC) [26] was installed in the HERA tunnel at $\theta = 0$ degrees and at $Z = 106\,\text{m}$ from the interaction point in the proton-beam direction. The FNC, a lead-scintillator calorimeter, had an energy resolution for hadrons $\sigma(E)/E = 0.70/\sqrt{E}$, with E in GeV, as measured in a test beam. The calorimeter was segmented vertically into 14 towers. Three planes of veto counters were located in front of the FNC to reject events in which a particle showered in inactive material along the beamline upstream of the FNC.

The luminosity was measured from the rate of the bremsstrahlung process $ep \to e\gamma p$. The resulting small angle energetic photons were measured by the luminosity monitor [27], a lead-scintillator calorimeter placed in the HERA tunnel at $Z = -107$ m.

3 Kinematics and cross sections

Figure 1 illustrates semi-inclusive leading-proton production in ep collisions. Four kinematic variables are needed to describe the reaction $e^+p \to e^+Xp$. They are defined in terms of the four-momenta of the incoming and outgoing positron, k and k', and of the incoming and outgoing proton, P and P', respectively.

The Lorentz-invariant kinematic variables used in inclusive studies are $Q^2 = -q^2 = -(k-k')^2$, the virtuality of the exchanged photon; $x = Q^2/(2P\cdot q)$ and $y = q\cdot P/(k\cdot P) \simeq Q^2/(sx)$; $W^2 = (P+k-k')^2 = m_p^2 + Q^2(1-x)/x$, the square of the photon-proton center-of-mass energy. In these equations, m_p is the mass of the proton and $\sqrt{s} = 300$ GeV is the e^+p center-of-mass energy. Among these variables, only two are independent.

Two additional variables are required to describe the leading proton. They are chosen as the momentum fraction carried by the outgoing proton

$$x_L = \frac{P'\cdot k}{P\cdot k}$$

and its transverse momentum with respect to the direction of the incoming proton, p_T. In terms of these variables, the square of the four-momentum transfer from the target proton is given by

$$t = (P - P')^2 \simeq -\frac{p_T^2}{x_L} - \frac{(1-x_L)^2}{x_L} m_p^2,$$

where the second term is the minimum kinematically-allowed value of $|t|$ for a given x_L. The variable t is the square of the four-momentum of the exchanged particle.

The differential cross section for inclusive $e^+p \to e^+X$ scattering, in the Q^2 region of this analysis, is written in terms of the proton structure function, $F_2(x, Q^2)$, as

$$\frac{d^2\sigma_{e^+p\to e^+X}}{dxdQ^2} = \frac{4\pi\alpha^2}{xQ^4}\left(1 - y + \frac{y^2}{2}\right) F_2(x, Q^2)(1+\Delta), \tag{1}$$

where Δ is a correction that takes into account the contribution of the longitudinal structure function, F_L, and of electroweak radiative effects. Similarly, the differential cross section for semi-inclusive leading-proton (LP) production can be written in terms of the leading-proton structure function $F_2^{\mathrm{LP}(4)}$,

$$\frac{d^4\sigma_{e^+p\to e^+Xp}}{dxdQ^2dx_Ldp_T^2} = \frac{4\pi\alpha^2}{xQ^4}\left(1 - y + \frac{y^2}{2}\right) F_2^{\mathrm{LP}(4)}(x, Q^2, x_L, p_T^2)(1+\Delta_{\mathrm{LP}}), \tag{2}$$

where Δ_{LP} is the analogue of Δ.

The structure function, $F_2^{\mathrm{LP}(4)}$ corresponds to the proton-to-proton fracture function $M_2^{p/p}(x, Q^2, x_L, p_T^2)$ [15], i.e. the structure function of a proton probed under the condition that the target fragmentation region contains a proton with a given x_L and p_T^2.

4 Reconstruction of the kinematic variables

In the Q^2 range of this analysis, the DIS events are characterized by the presence of a scattered positron, mostly in RCAL. The scattered positron was reconstructed using an electron finder algorithm based on a neural network [28].

The properties of the hadronic final state in the central detector were derived using the energy flow objects (EFOs) [29] reconstructed from CAL clusters and CTD tracks by combining the CTD and CAL information to optimize the resolution of the reconstructed kinematic variables. The EFOs were additionally corrected for energy loss due to inactive material in front of the CAL.

The DIS variables x, y, Q^2 and W were obtained by using a weighting method [30], which uses a weighted average of the values determined from the electron [31] and double-angle [32] methods. The variable y was also reconstructed using the Jacquet-Blondel method [33], which uses information from the hadronic final state to reconstruct the event kinematics, and is denoted by $y_{\rm JB}$.

The momentum $p = (p_X, p_Y, p_Z)$ of the leading-proton candidate was determined using the LPS. The variable x_L was evaluated as $x_L = p_Z/E_p$ and the squared transverse momentum as $p_T^2 = p_X^2 + p_Y^2$.

5 The data sample and the event selection

During 1997, the ZEUS detector collected an integrated luminosity of 27.8 pb^{-1}. However, the amount of data recorded when the experimental conditions allowed the LPS to be operational correspond to an integrated luminosity of 12.8 pb^{-1}. Out of this sample, 4.8 pb^{-1} of data were collected with all the LPS stations. In the remaining part, only the spectrometer s456 was used.

Online, a three-level trigger [34] was used. At the third level, the event variables were reconstructed with an accuracy close to that obtained offline. Final detector calibration and full-event reconstruction were performed offline.

Two sets of events were selected [35], the inclusive DIS sample and the LPS sample. For a fraction of the inclusive DIS candidate events the trigger was prescaled, thus reducing the effective integrated luminosity of the inclusive DIS sample to 1 pb^{-1}. The selection of the LPS sample was performed with a dedicated LPS trigger.

The presence of a good positron candidate in the CAL was required in the trigger chain used to select the inclusive DIS sample. In addition the following conditions were applied:

- $|Z_{\rm vtx}| < 50$ cm, where $Z_{\rm vtx}$ is the Z coordinate of the event vertex. This cut is needed to remove background due to proton beam-gas interactions and cosmic rays;
- energy of the scattered positron $E'_e > 10$ GeV. The positron position was required to be outside the region close to the rear beampipe hole, where the presence of inactive material reduced the precision of the energy measurement;
- the quantity $E - P_Z$, where the energy E and the longitudinal momentum P_Z are summed over all the EFOs and the scattered positron, in the range $38 < E - P_Z < 65$ GeV, to exclude background from photoproduction, proton beam-gas interactions and cosmic rays;
- $y_{\rm JB} > 0.03$ in order to ensure hadronic activity away from the forward direction.

The following cuts define the kinematic domain:

- $Q^2 > 3$ GeV^2, to select DIS events with large virtuality of the exchanged photon;

- $45 < W < 225$ GeV, to ensure a wide kinematic coverage of the hadronic system.

The number of events that passed the inclusive DIS selection cuts was 145447.

The LPS sample was selected from the DIS sample, by requiring in addition the LPS trigger and the following conditions:

- a reconstructed track in the LPS with $p_T^2 < 0.5$ GeV^2 and $x_L > 0.32$. To reduce the sensitivity of the LPS acceptance due to the uncertainties of the location of the beampipe elements, a cut was applied to the minimum distance, Δ_{pipe}, between the track and the beampipe requiring $\Delta_{\text{pipe}} > 0.04\,(0.25)$ cm for s456 (s123). The selection of tracks with $\Delta_{\text{pot}} > 0.02$ cm, where Δ_{pot} is the minimum distance of the track from the edge of any LPS detector, ensured that the tracks were well within the active regions of the silicon detectors;
- the sum of the energy and the longitudinal momentum of both the energy deposits in the CAL and the particle detected in the LPS, $E+P_Z$, was required to be smaller than 1655 GeV; this cut rejected most of the random overlays of DIS events with protons from the beam-halo or from a proton-gas collision.

A total of 73275 events survived the above selection criteria, of those 6008 had a track in s123 and 67267 had a track in s456.

6 Monte Carlo simulation

To determine the acceptance of the apparatus, inclusive DIS events with $Q^2 > 0.5$ GeV^2 were generated using DJANGOH [37], which is interfaced to HERACLES [38] for electroweak radiative effects. In order to study the migration of events from low Q^2, a sample of photoproduction events with $Q^2 < 0.5$ GeV^2 was generated with PYTHIA [39]. In the MC samples, the hadronic final state was generated using the Matrix Element Parton Shower model (MEPS) [40] for QCD radiation and JETSET [41] for hadronization. The diffractive events in DJANGOH were generated using the soft-color-interaction mechanism [14].

All the MC events were passed through the standard simulation of the ZEUS detector, based on GEANT v3.13 [42], and trigger and through the same reconstruction and analysis programs as the data. The simulation included the geometry of the beampipe apertures, the magnetic field along the leading-proton trajectory and the proton-beam emittance.

To obtain a good description of the data, it was necessary to reweight the leading-proton x_L and p_T^2 distributions generated by the MC [35, 43]; the fraction of diffractive events with respect to the total was also reweighted in bins of x_L. In particular, the slope of the exponential p_T^2 distribution was increased by a constant value $\Delta b = 3.4$ GeV^{-2}

and the x_L spectrum was reweighted to a flat distribution below the diffractive peak. The reweighting parameters were chosen according to previous measurements [7]. The reweighting preserved the total MC cross section.

For the LPS sample, the comparison between the data and the sum of the reweighted MC samples (DJANGOH and PYTHIA), for the DIS variables and the LPS specific variables, is shown in Figs. 2 and 3. The agreement is generally good. The LPS variable Δ_{pipe} is not perfectly reproduced by the reweighted MC, but the selection cut applied is far from the region in which the disagreement is observed.

7 Acceptance

The acceptance was defined as the ratio of the number of reconstructed events in a bin to the number of generated events in that bin. This definition includes the effects of the geometrical acceptance of the apparatus, its efficiency and resolution, and the event selection efficiency. Figure 4 shows the acceptances of the LPS station combinations s123 and s456 as a function of x_L and p_T^2. The maximum acceptance is 10% in the region $0.63 < x_L < 0.65$, $0.05 < p_T^2 < 0.1$ GeV^2 for the spectrometer s123 and 52% in the region $0.77 < x_L < 0.8$, $p_T^2 < 0.05$ GeV^2 for the spectrometer s456.

The analysis bins were chosen according to the LPS acceptance, resolution (Section 2) and available statistics.

For completeness, also shown in Fig. 4 are the limits of integration over p_T^2 used for the cross section measurements.

8 Background studies

The LPS data sample contains three background contributions,

- non-baryon contributions;
- overlay events;
- misidentified low-Q^2 background.

The LPS has no particle identification capability, but MC studies indicate that most high-x_L particles in the LPS are protons. The MC expectations were tested with a subsample of LPS-tagged events where a neutron candidate was found in the FNC [36]. The neutron candidate was required to have a minimum energy deposit of 50 GeV and the total $E+P_Z$ of the event, including the neutron, was required to be below 1750 GeV. A total of 47 events was found. For this class of events the track in the LPS is most likely either a π^+ or a K^+. Figure 5a shows the ratio $\rho_{\rm FNC}$ of the LPS-FNC tagged events to the LPS tagged ones as a function of x_L. The reweighted MC describes the data well and therefore can be used to subtract the background. The fraction R of events with a positive meson reconstructed in the LPS, evaluated with the reweighted MC, is shown in Fig. 5b as a function of x_L. The fraction R in the MC was found to be independent of p_T^2. It is substantial at low x_L and falls below 10% above $x_L \approx 0.6$. This contribution was subtracted.

The $E + P_Z$ spectrum for the beam-halo events was constructed as a combination of generic DIS events and a beam-halo track reconstructed in the LPS in randomly triggered events. The $E+P_Z$ distribution was normalized to the data for $E+P_Z > 1685$ GeV, which mainly contain beam-halo events. The background remaining after the $E + P_Z < 1655$ GeV cut was negligible for $x_L < 0.9$, and reached $(8 \pm 3)\%$ for $x_L > 0.98$. The expected fraction of overlay events was subtracted.

The acceptance corrections were calculated using the MC generated with $Q^2 > 2$ GeV^2. The contribution of events which migrate from the region $Q^2 < 2$ GeV^2 was found to be independent of x_L and p_T^2 and equal to $(7.3 \pm 0.5)\%$ and was subtracted.

9 Systematic studies

The systematic uncertainties were calculated by varying the cuts and by modifying the analysis procedure. The stability of the DIS selection was checked by varying the selection cuts by an amount which in most cases was conservatively taken to be larger than the resolution of the corresponding variable,

- the $|Z_{\rm vtx}|$ cut was varied by ± 10 cm;
- the cut on the scattered positron energy was varied by $\pm$ 2 GeV and the width of the fiducial region in the rear calorimeter was varied by 0.5 cm in the X and Y directions;
- the $E - P_Z$ cut was changed to $35 < E - P_Z < 68$ GeV and $41 < E - P_Z < 62$ GeV;
- the $y_{\rm JB}$ cut was raised to 0.04.

The observed changes in the cross section were below 1% and were neglected. The variation in the LPS selection of the $\Delta_{\rm pipe}$ threshold by $\pm$ 0.03 cm and the $\Delta_{\rm pot}$ threshold by $\pm$ 0.01, led to negligible changes in the cross section (<1%).

The following checks resulted in non-negligible systematic uncertainties of the cross section (the mean value is given in brackets):

- the reweighting parameter Δb was varied by ± 0.9 GeV^{-2}, compatible with the spread of b versus x_L ($^{+6.8\%}_{-5.9\%}$);
- the subtracted fraction of background from π^+ and K^+ reconstructed in the LPS was varied by the statistical uncertainty derived from the LPS-FNC data (see Fig. 5) ($^{+1.7\%}_{-1.7\%}$ for $x_L < 0.7$);
- the fraction of overlay events to be subtracted from the data was increased and decreased by its statistical uncertainty ($^{+2.0\%}_{-2.0\%}$ for $x_L > 0.9$);
- the uncertainty on the beam optics was evaluated by varying in the MC simulation the transverse momentum spread of the proton beam by $\pm$ 10% [17], leading to a change of typically $\pm 1.4\%$. In addition, the positions of the LPS stations were varied to reflect the actual position of the stations during the data taking period. This was done because, in the simulation, the MC assumes only one average position ($^{+2.5\%}_{-1.8\%}$). In the diffractive region the uncertainty related to the beam optics increases to $\pm 10\%$.

The resulting total systematic uncertainty, obtained by adding in quadrature all the individual systematic uncertainties (combining positive and negative contributions, separately), excluding an overall normalization uncertainty of 2% from the luminosity measurement, is shown in the figures as error band, that includes both a correlated and a non-correlated component.

10 Results

All measurements were performed separately for the s123 and s456 spectrometers, and were then combined in a weighted average, using only statistical uncertainties. This procedure was repeated for every systematic check.

Some measurements are presented as normalized to the cross section, σ_{tot}, determined from the inclusive DIS sample described in Section 5.

All cross section measurements are averaged over a given bin and quoted at the mean value of the variable in that bin.

The measurements for $x_L > 0.93$ are presented here in a different kinematic domain than those previously published [17].

10.1 Transverse-momentum spectra and p_T^2 slopes

The double-differential cross section $d^2\sigma_{\text{LP}}/dx_L dp_T^2$ as a function of p_T^2 in bins of x_L is presented in Fig. 6 and given in Table 1. The results obtained with the s123 and s456 spectrometers are shown separately. Within the uncorrelated uncertainties, the two samples lead to consistent results. The lines shown in Fig. 6 represent the results of a fit of an exponential function $A \cdot e^{-bp_T^2}$ to the combined cross section $d^2\sigma_{\rm LP}/dx_L dp_T^2$. The band shows the statistical uncertainty of the fit. The slopes are presented as a function of x_L in Fig. 7 and given in Table 2. The slopes show no strong dependence on x_L. The mean value of the slopes is $\langle b \rangle = 6.76 \pm 0.07(\text{stat.})^{+0.63}_{-0.52}(\text{syst.})$ GeV^{-2}. The measurements of the p_T^2-slopes at $\langle Q^2 \rangle = 5.1$ GeV^2 and $\langle Q^2 \rangle = 30.1$ GeV^2, in the range $45 < W < 225$ GeV, where x_L bins were combined, are presented in Fig. 8 and given in Table 3. Also shown are the ZEUS 1994 data [16] in the range $Q^2 < 0.02$ GeV^2 and $176 < W < 225$ GeV and the ZEUS 1995 [7] data in the range $0.1 < Q^2 < 0.74$ GeV^2 and $85 < W < 258$ GeV. The p_T^2-slopes are independent of the virtuality of the exchanged photon.

10.2 Longitudinal-momentum spectra

The cross section as a function of x_L has been measured in three bins of p_T^2: $0 < p_T^2 < 0.04$, $0.04 < p_T^2 < 0.15$ and $0.15 < p_T^2 < 0.5$ GeV^2. The leading-proton production rate, $1/\sigma_{\rm tot} \cdot d\sigma_{\rm LP}/dx_L$, for the three p_T^2 ranges is shown in Fig. 9 and listed in Table 4. Due to the LPS acceptance, the accessible x_L range changes as a function of p_T^2, as seen in the figure. The rate as a function of x_L is approximately flat up to the diffractive peak, where it increases by a factor of about six. This behavior of the cross section as a function of x_L is essentially independent of p_T^2.

Since, as discussed in the previous section, also the p_T^2-slopes are independent of x_L, the cross section as a function of x_L can be extrapolated to the full $x_L > 0.32$ and $p_T^2 > 0.5$ GeV^2 range. The measurement of $1/\sigma_{\rm tot} \cdot d\sigma_{\rm LP}/dx_L$ as a function of x_L, extrapolated to the full $p_T^2 < 0.5$ GeV^2 range is shown in Fig. 10 and given in Table 5. For comparison, the ZEUS 1995 data [7] from a lower Q^2 are also shown. The two measurements are consistent.

For $p_T^2 < 0.04$ GeV^2, the measurement of $1/\sigma_{\rm tot} \cdot d\sigma_{\rm LP}/dx_L$ can also be compared to previous measurements in the photoproduction regime ($Q^2 < 0.02$ GeV^2) [7]. The comparison is shown in Fig. 11. Due to the low p_T^2 values, the diffractive peak is not accessible 4. The photoproduction data tend to lie systematically below the higher Q^2 measurement, though within uncertainties the results are consistent.

10.3 Rates of leading proton production to inclusive DIS

The rate of leading-proton production, $r^{\rm LP(3)}(x, Q^2, x_L)$, in e^+p scattering was determined as

$$r^{\mathrm{LP}(3)}(x,Q^2,x_L)=\frac{N^{\mathrm{LPS}}(x,Q^2,x_L)}{N^{\mathrm{DIS}}(x,Q^2)}\frac{A_{\mathrm{DIS}}}{A_{\mathrm{LPS}}}\frac{\mathcal{L}^{\mathrm{DIS}}}{\mathcal{L}^{\mathrm{LPS}}}\frac{1}{\Delta x_L}, \tag{3}$$

where $N^{\mathrm{LPS}}(x,Q^2,x_L)$ is the number of events corresponding to an integrated luminosity $\mathcal{L}^{\mathrm{LPS}}$, with a proton candidate in the LPS in a given x, Q^2, x_L bin and integrated over $0 < p_T^2 < 0.5$ GeV^2, and $N^{\mathrm{DIS}}(x,Q^2)$ is the number of DIS events corresponding to an integrated luminosity $\mathcal{L}^{\mathrm{DIS}}$, in that x, Q^2 bin. The acceptance A_{DIS} was estimated by applying only the DIS selection cuts and the acceptance A_{LPS} corrects for the leading-proton selection. The variable Δx_L indicates the size of the x_L bin.

The ratio $r^{\mathrm{LP}(3)}$ as a function of x_L in bins of x and Q^2 is shown in Fig. 12 and given in Table 6. The x_L range of the measurement is limited to $0.32 < x_L < 0.92$, as detailed studies of the diffraction region were presented elsewhere [17]. The ratio $r^{\mathrm{LP}(3)}$ has also been measured in the three ranges of p_T^2 and the values are given in Tables 7, 8 and 9. The $r^{\mathrm{LP}(3)}$ values are approximately constant over the kinematic range of this analysis, independently of the p_T^2 range.

The rate of leading-proton production as a function of x and Q^2, integrated over $0.32 < x_L < 0.92$ and $p_T^2 < 0.5$ GeV^2, $r^{\mathrm{LP}(2)}(x,Q^2)$, is shown in Fig. 13 and given in Table 10. The ratio $r^{\mathrm{LP}(2)}$ is approximately constant as a function of x and of Q^2. The mean value $\langle r^{\mathrm{LP}(2)}\rangle = 0.240 \pm 0.001(\mathrm{stat.})^{+0.020}_{-0.018}(\mathrm{syst.})$ means that approximately 24% of inclusive DIS events with $p_T^2 < 0.5$ GeV^2 have a leading proton in the range $0.32 < x_L < 0.92$.

The ratio $\langle r^{\mathrm{LP}(2)}\rangle$ averaged over x as a function of Q^2 is shown in Fig. 14 and given in Table 11, in the range $0.32 < x_L < 0.92$, $p_T^2 < 0.5$ GeV^2 and $45 < W < 225$ GeV. A slight increase with Q^2 can not be excluded. To further investigate the Q^2 dependence, the rates integrated over $0.6 < x_L < 0.97$ can be compared to the equivalent rates for $\langle Q^2\rangle = 0.29$ GeV^2 measured by ZEUS previously [7]. The result is shown in Fig. 14 and included in Table 11. Assuming that the systematic uncertainties have a similar origin, dominated by the LPS acceptance, a steady rise with Q^2 is observed. A similar effect was observed in leading-neutron production [36], where it was attributed to absorption and rescattering effects [44], which disappear when the transverse size of the virtual photon decreases with increasing Q^2.

10.4 The leading-proton structure functions

The ratio $r^{\mathrm{LP}(2)}$ can be expressed as the ratio of $F_2^{\mathrm{LP}(2)}$ to F_2,

$$r^{\mathrm{LP}(2)}(x,Q^2)=\frac{F_2^{\mathrm{LP}(2)}(x,Q^2)}{F_2(x,Q^2)}, \tag{4}$$

where $F_2^{\mathrm{LP}(2)}$ is obtained from $F_2^{\mathrm{LP}(4)}$ by integrating over x_L and p_T^2. Therefore, the values of $F_2^{\mathrm{LP}(2)}$ can be obtained from the measured $r^{\mathrm{LP}(2)}$ and F_2. The values of F_2 were obtained from the NLO ZEUS-S fit parametrization of the parton distribution of the proton [45].

The structure function $F_2^{\mathrm{LP}(2)}$ is presented in Fig. 15, plotted as a function of x at fixed Q^2 values for $0.32 < x_L < 0.92$, $p_T^2 < 0.5$ GeV^2 and given in Table 12. The curves in the plot show the F_2 parametrization scaled by the average value $\langle r^{\mathrm{LP}(2)} \rangle = 0.24$ and the bands represent the one-standard-deviation limits of the NLO ZEUS-S parametrization. A very good description of $F_2^{\mathrm{LP}(2)}$ is obtained, as expected from $r^{\mathrm{LP}(2)}$ being independent of x and Q^2.

10.5 Comparison to leading neutrons

The rate of leading-proton production can be compared to the recent measurement of leading neutrons [36] for p_T^2 <0.04 GeV^2. The comparison is shown in Fig. 16.

In the range $0.32 < x_L < 0.92$, there are approximately twice as many protons as neutrons. This is consistent with the additive quark model [46], in which the probabilities to have a proton or a neutron in the final state are 2/3 and 1/3, respectively. In a particle exchange model, the exchange of isovector particles would result in half as many protons as neutrons. Thus, exchange of isoscalars must be invoked to account for the observed proton rate [13]. This contribution is likely also to explain the different behavior of the rates at large x_L.

The slopes of the p_T^2 distributions for leading protons and neutrons are shown in Fig. 17. Although the p_T^2 and Q^2 ranges are different, the two samples have similar values of b in the region $0.65 < x_L < 0.8$, where pion exchange is expected to dominate the production mechanism [13].

10.6 Comparison to models

The predictions of the model of Szczurek et al. [13] are compared to the leading-proton production rate $1/\sigma_{\mathrm{tot}} \cdot d\sigma_{\mathrm{LP}}/dx_L$ and the p_T^2-slopes in Fig. 18. In this model, leading-proton production for $0.6 < x_L < 0.9$ is dominated by isoscalar Reggeon exchange. Diffractive processes due to Pomeron exchange become increasingly important as x_L approaches unity. The contribution of pion exchange plays an important role in the medium x_L range. The model describes reasonably well the shape of the longitudinal momentum spectrum and of the p_T^2-slopes. The normalization of the Reggeon contribution, which has a large theoretical uncertainty [13], may be constrained by this measurement.

In Fig. 19 various DIS Monte Carlo models are compared to the experimental data. The prediction of Djangoh [37] with SCI [40] and Rapgap [47] are compared to the leading-proton production rate $1/\sigma_{\rm tot} \cdot d\sigma_{\rm LP}/dx_L$ and the p_T^2-slopes. In both MC models, the QCD radiation was performed either by parton shower [40] or color dipole model (CDM) [48]. None of the DIS Monte Carlo models can reproduce the flat dependence of x_L below the diffractive peak. The MC generator Djangoh, with SCI and MEPS, reproduces quite well the dependence of b on x_L, although the mean values of the slope are lower than the measured ones. In the other MC models, the value of the slope is consistent with the measurements only at high x_L.

11 Summary

The cross section for leading-proton production for $x_L > 0.32$ and $p_T^2 < 0.5$ GeV^2 and its rate to the inclusive DIS cross section have been measured in the range $Q^2 > 3$ GeV^2 and $45 < W < 225$ GeV, with 12.8 pb^{-1} collected during 1997 with the ZEUS leading-proton spectrometer. The leading-proton production cross section as a function of p_T^2 falls exponentially with a mean slope $\langle b \rangle = 6.76 \pm 0.07(\text{stat.})^{+0.63}_{-0.52}(\text{syst.})$ GeV^{-2}, approximately independent of x_L and of the photon virtuality Q^2. Below the diffractive peak, the x_L distribution is flat, independent of p_T^2 and Q^2. The ratios $r^{\rm LP(2)}$ and $r^{\rm LP(3)}$ show no strong dependence on x or Q^2. In the range $0.32 < x_L < 0.92$ and $p_T^2 < 0.5$ GeV^2, approximately 24% of DIS events have a leading proton. The ratio $\langle r^{\rm LP(2)} \rangle$ averaged over x is rising very slowly with Q^2 in the DIS regime. This trend is further confirmed by measurements at lower Q^2. The dependence of the leading-proton structure functions $F_2^{\rm LP(2)}$ on x and Q^2 is approximately the same as that of F_2.

The comparisons with the leading-neutron production in DIS show that the yield of leading-proton production is almost twice that of the leading neutron one. The p_T^2-slopes have a different dependence on x_L, but are compatible in the range $0.65 < x_L < 0.8$, where pion-exchange is dominant.

The main features of the experimental data are reproduced by a Regge-inspired model. The results of this study are an important ingredient in modelling the leading particle production in hadron-hadron interactions, which is not properly reproduced by existing generators.

Acknowledgments

We thank the DESY Directorate for their encouragement, and gratefully acknowledge the support of the DESY computing and network services. We are specially grateful to the HERA machine group: collaboration with them was crucial to the successful installation and operation of the leading proton spectrometer. The design, construction and installation of the ZEUS detector have been made possible by the ingenuity and effort of many people from DESY and home institutes who are not listed as authors. Finally, it is a pleasure to thank F. A. Ceccopieri and L. Trentadue for many useful discussions.

References

[1] R. P. Feynman Phys. Rev. **23**, 1415 (1969).

[2] M. Basile et al., Nuovo Cimento **66A**, 129 (1981);
M. Basile et al., Lettere al Nuovo Cimento **32**, 321 (1981).

[3] V.N. Gribov et al., *The creation of QCD and the effective energy*, L.N. Lipatov (ed.), World Scientific Series in 20th Century Physics, Vol. 25, World Scientific, Singapore (2001).

[4] J. Whitmore and M. Derrick, Phys. Lett. **B 50**, 280 (1974).

[5] A. E. Brenner et al., Phys. Rev. **D 26**, 1497 (1982).

[6] M. Aguilar-Benitez et al., Z. Phys. **C 50**, 405 (1991).

[7] ZEUS Collab., S. Chekanov et al., Nucl. Phys. **B 685**, 3 (2003).

[8] H1 Collab., C. Adloff et al., Eur. Phys. J. **C 6**, 587 (1999);
H1 Collab., C. Adloff et al., Nucl. Phys. **B 619**, 3 (2001).

[9] J. D. Sullivan, Phys. Rev. **D 5**, 1732 (1972).

[10] R. Zoller, Z. Phys. **C 53**, 443 (1992).

[11] H. Holtmann et al., Phys. Lett. **B 338**, 363 (1994).

[12] B. Kopeliovich, B. Povh and I. Potashnikova, Z. Phys. **C 73**, 125 (1996).

[13] A. Szczurek, N.N. Nikolaev and J. Speth, Phys. Lett. **B 428**, 383 (1998).

[14] A. Edin, G. Ingelman and J. Rathsman, Phys. Lett. **B 366**, 371 (1996).

[15] L. Trentadue and G. Veneziano, Phys. Lett. **B 323**, 210 (1994);
D. Graudenz, Nucl. Phys. **B 432**, 351 (1994);
L. Trentadue, Nucl. Phys. Proc. Suppl. **39**, 50 (1995);
L. Trentadue, Nucl. Phys. Proc. Suppl. **64**, 152 (1998);
D. de Florian and R. Sassot, Phys. Rev. **D 56**, 426 (1997);
D. de Florian and R. Sassot, Phys. Rev. **D 58**, 054003 (1998).

[16] ZEUS Collab., M. Derrick et al., Z. Phys. **C 73**, 253 (1997).

[17] ZEUS Collab., S. Chekanov et al., Eur. Phys. J. **C 38**, 43 (2004).

[18] M.T. Dovaa and S. Ferrari, Eur. Phys. J. **C 52**, 673 (2007).

[19] R.S. Fletcher, T.K. Gaisser, P. Lipari, T. Stanev, Phys. Rev. **D 50**, 5710 (1994).

[20] N.N. Kalmykov, S.S. Ostapchenko, A.I. Pavlov, Nucl. Phys. Proc. Suppl. **B 52**, 17 (1997).

[21] ZEUS Collab., U. Holm (ed.), *The ZEUS Detector*, Status Report (unpublished) DESY, 1993, available on `http://www-zeus.desy.de/bluebook/bluebook.html`.

[22] N. Harnew et al., Nucl. Instr. and Meth. **A 279**, 290 (1989);
B. Foster et al., Nucl. Phys. Proc. Suppl. **B 32**, 181 (1993);
B. Foster et al., Nucl. Instr. and Meth. **A 338**, 254 (1994).

[23] M. Derrick et al., Nucl. Instr. and Meth. **A 309**, 77 (1991);
A. Andresen et al., Nucl. Instr. and Meth. **A 309**, 101 (1991);
A. Caldwell et al., Nucl. Instr. and Meth. **A 321**, 356 (1992);
A. Bernstein et al., Nucl. Instr. and Meth. **A 336**, 23 (1993).

[24] A. Bernstein et al., Nucl. Instr. and Meth. **A 336**, 33 (1993).

[25] A. Dwuraźny et al., Nucl. Instr. and Meth. **A 277**, 176 (1989).

[26] S. Bhadra et al., Nucl. Instr. and Meth. **A 354**, 479 (1995);
ZEUS Collab., FNC group, S. Bhadra et al., Nucl. Instr. and Meth. **A 394**, 121 (1997);
ZEUS FNC Group, S. Bhadra et al., *Proc. of the Seventh International Conference on calorimetry in High Energy Physics, Tuscon, Arizona, November 1997*, E. Cheu et al. (ed.), p. 295.

[27] J. Andruszków et al., Preprint DESY-92-066, DESY, 1992;
ZEUS Collab., M. Derrick et al., Z. Phys. **C 63**, 391 (1994);
J. Andruszków et al., Acta Phys. Pol. **B 32**, 2025 (2001).

[28] H. Abramowicz, A. Caldwell and R. Sinkus, Nucl. Instr. and Meth. **A 365**, 508 (1995).

[29] ZEUS Collab., J. Breitweg et al., Eur. Phys. J. **C 1**, 81 (1998);
ZEUS Collab., J. Breitweg et al., Eur. Phys. J. **C 6**, 43 (1999);
G. Briskin, PhD Thesis, Tel Aviv University (1998), report DESY-THESYS-1998-036.

[30] ZEUS Collab., S. Chekanov et al., Nucl. Phys. **713**, 3 (2005).

[31] ZEUS Collab., J. Breitweg et al., Phys. Lett. **B 407**, 432 (1997).

[32] S. Bentvelsen, J. Engelen and P. Kooijman, *Proceedings of the Workshop on Physics at HERA*, Volume 1, W. Buchmüller and G. Ingelman (eds.), DESY (1991) p. 23;
K. C. Hoeger, ibid., p. 43.

[33] F. Jacquet e A. Blondel, *Proceedings of the Study of an ep facility for Europe*, U. Amaldi (ed.), DESY 79/48, 391.

[34] W.H. Smith, K. Tokushuku and L.W. Wiggers, *Proc. of int. conference "Computing in High Henergy Physics" (CHEP'92)*, Annecy, France, Sept. 1992. Also in DESY 92-150.

[35] L. Rinaldi, Ph.D. thesis, University of Bologna (2006), Report DESY-THESIS-2006-028.

[36] ZEUS Collab., S. Chekanov et al., Nucl. Phys. **776**, 1 (2007).

[37] G. A. Schüler and H. Spiesberger, *Proceedings of the Workshop on Physics at HERA*, Volume 3, W. Buchmüller and G. Ingelman (eds.), DESY (1991), p. 1419;
H. Spiesberger, DJANGOH, `http://www.desy.de/~hspiesb/djangoh.html`.

[38] A. Kwiatkowski, H. Spiesberger and H.-J. Möhring, in *Proceedings of the Workshop on Physics at HERA*, Volume 3, W. Buchmüller and G. Ingelman (eds.), DESY (1991), p. 1294.

[39] T. Sjöstrand et al., Comp. Phys. Comm. **135**, 238 (2001).

[40] G. Ingelman, A. Edin and J. Rathsman, Comp. Phys. Comm. **101**, 108 (1997).

[41] T. Sjöstrand and M. Bengtsson, Comp. Phys. Comm. **43**, 367 (1987);
T. Sjöstrand, Comp. Phys. Comm. **82**, 74 (1994).

[42] R. Brun et al., *GEANT3* , Technical Report CERN DD/EE/84-1, CERN, 1987.

[43] G. Bruni, G Iacobucci, L. Rinaldi, M. Ruspa, *Proceedings of the HERA-LHC workshop (CERN-2005-014)*, 605 (2005).

[44] N. N. Nikolaev et al., Phys. Rev. **D 60**, 014004 (1999);
U. D'Alesio and H.J. Pirner, Eur. Phys. J. **A 7**, 109 (2000);
A.B. Kaidalov et. al., Eur. Phys. J. **C 47**, 385 (2006);
V.A. Khoze, A.D. Martin and M.G. Ryskin, Eur. Phys. J. **C 48**, 797 (2006).

[45] ZEUS Collab., S. Chekanov et al., Eur. Phys. J. **C 42**, 13 (2005).

[46] E. M. Levin, L. L. Frankfurt, JETP Lett.**2**, 65 (1965).

[47] H. Jung, Comp. Phys. Comm. **85**, 147 (1995).

[48] L. Lönnblad, Comp. Phys. Comm. **71**, 15 (1992).

x_L range	p_T^2 range (GeV^2)	$d^2\sigma_{\rm LP}/dx_L dp_T^2$ s123 (nb/GeV^2)	$d^2\sigma_{\rm LP}/dx_L dp_T^2$ s456 (nb/GeV^2)	$d^2\sigma_{\rm LP}/dx_L dp_T^2$ Combined (nb/GeV^2)
0.32-0.38	0.00-0.05	$467 \pm 40^{+49}_{-53}$		$467 \pm 40^{+49}_{-53}$
	0.05-0.10	$387 \pm 68^{+45}_{-161}$		$387 \pm 68^{+45}_{-161}$
0.38-0.44	0.00-0.05	$367 \pm 28^{+32}_{-22}$	$502 \pm 41^{+42}_{-83}$	$409 \pm 23^{+28}_{-31}$
	0.05-0.10	$349 \pm 46^{+35}_{-57}$		$349 \pm 46^{+35}_{-57}$
0.44-0.50	0.00-0.05	$362 \pm 25^{+18}_{-40}$	$469 \pm 25^{+46}_{-49}$	$415 \pm 18^{+20}_{-36}$
	0.05-0.10	$332 \pm 40^{+19}_{-38}$		$332 \pm 40^{+19}_{-38}$
	0.10-0.15	$165 \pm 44^{+22}_{-51}$		$165 \pm 44^{+22}_{-51}$
0.50-0.56	0.00-0.05	$403 \pm 26^{+21}_{-26}$	$463 \pm 22^{+128}_{-14}$	$437 \pm 17^{+44}_{-12}$
	0.05-0.10	$317 \pm 33^{+51}_{-17}$	$298 \pm 19^{+52}_{-16}$	$303 \pm 17^{+41}_{-12}$
	0.10-0.15	$219 \pm 47^{+40}_{-13}$		$219 \pm 47^{+40}_{-13}$
0.56-0.62	0.00-0.05	$460 \pm 33^{+22}_{-70}$	$463 \pm 19^{+30}_{-26}$	$462 \pm 16^{+20}_{-31}$
	0.05-0.10	$303 \pm 27^{+29}_{-25}$	$306 \pm 16^{+16}_{-30}$	$305 \pm 13^{+16}_{-23}$
	0.10-0.15	$178 \pm 35^{+42}_{-14}$	$210 \pm 17^{+8}_{-46}$	$204 \pm 15^{+7}_{-36}$
	0.15-0.20		$136 \pm 22^{+40}_{-11}$	$136 \pm 22^{+40}_{-11}$
0.62-0.65	0.00-0.05	$410 \pm 53^{+28}_{-56}$	$463 \pm 20^{+19}_{-17}$	$456 \pm 19^{+17}_{-19}$
	0.05-0.10	$296 \pm 29^{+18}_{-12}$	$324 \pm 31^{+16}_{-51}$	$309 \pm 21^{+12}_{-22}$
	0.10-0.15	$189 \pm 43^{+19}_{-51}$	$187 \pm 16^{+13}_{-16}$	$187 \pm 15^{+12}_{-18}$
	0.15-0.20		$148 \pm 17^{+8}_{-27}$	$148 \pm 17^{+8}_{-27}$
	0.20-0.25		$134 \pm 22^{+8}_{-42}$	$134 \pm 22^{+8}_{-42}$
0.65-0.68	0.00-0.05	$421 \pm 74^{+64}_{-71}$	$464 \pm 16^{+27}_{-16}$	$462 \pm 16^{+27}_{-17}$
	0.05-0.10	$320 \pm 29^{+17}_{-43}$	$297 \pm 33^{+24}_{-66}$	$310 \pm 22^{+15}_{-52}$
	0.10-0.15	$181 \pm 36^{+81}_{-19}$	$298 \pm 37^{+20}_{-131}$	$238 \pm 26^{+11}_{-28}$
	0.15-0.20		$118 \pm 13^{+42}_{-6}$	$118 \pm 13^{+42}_{-6}$
	0.20-0.25		$119 \pm 16^{+18}_{-6}$	$119 \pm 16^{+18}_{-6}$
	0.25-0.35		$87 \pm 12^{+7}_{-15}$	$87 \pm 12^{+7}_{-15}$

Table 1: *The double differential cross section $d^2\sigma_{\rm LP}/dx_L dp_T^2$ as a function of x_L and p_T^2, separately measured with the spectrometers s123 and s456 and the combined result. Statistical uncertainties are listed first, followed by systematic uncertainties.*

Table 1 (cont.)

x_L range	p_T^2 range (GeV^2)	$d^2\sigma_{\rm LP}/dx_L dp_T^2$ s123 (nb/GeV^2)	$d^2\sigma_{\rm LP}/dx_L dp_T^2$ s456 (nb/GeV^2)	$d^2\sigma_{\rm LP}/dx_L dp_T^2$ Combined (nb/GeV^2)
0.68-0.71	0.00-0.05	$253 \pm 85^{+27}_{-134}$	$500 \pm 15^{+17}_{-17}$	$493 \pm 15^{+16}_{-28}$
	0.05-0.10	$320 \pm 29^{+22}_{-42}$	$366 \pm 41^{+24}_{-138}$	$335 \pm 24^{+17}_{-74}$
	0.10-0.15	$184 \pm 31^{+57}_{-17}$	$259 \pm 47^{+39}_{-55}$	$207 \pm 26^{+47}_{-15}$
	0.15-0.20	$92 \pm 41^{+40}_{-74}$	$155 \pm 24^{+40}_{-11}$	$139 \pm 21^{+33}_{-45}$
	0.20-0.25		$103 \pm 16^{+32}_{-7}$	$103 \pm 16^{+32}_{-7}$
	0.25-0.35		$85 \pm 10^{+6}_{-4}$	$85 \pm 10^{+6}_{-4}$
	0.35-0.50		$44 \pm 9^{+4}_{-9}$	$44 \pm 9^{+4}_{-9}$
0.71-0.74	0.00-0.05		$472 \pm 12^{+28}_{-13}$	$472 \pm 12^{+28}_{-13}$
	0.05-0.10	$279 \pm 27^{+59}_{-16}$	$255 \pm 24^{+51}_{-42}$	$266 \pm 18^{+49}_{-24}$
	0.10-0.15	$217 \pm 33^{+24}_{-38}$	$130 \pm 33^{+85}_{-16}$	$173 \pm 23^{+52}_{-15}$
	0.15-0.20	$114 \pm 43^{+34}_{-58}$	$250 \pm 66^{+51}_{-133}$	$154 \pm 36^{+25}_{-69}$
	0.20-0.25		$116 \pm 27^{+55}_{-15}$	$62 \pm 19^{+55}_{-15}$
	0.25-0.35		$86 \pm 16^{+11}_{-25}$	$86 \pm 16^{+11}_{-25}$
	0.35-0.50		$27 \pm 5^{+2}_{-2}$	$27 \pm 5^{+2}_{-2}$
0.74-0.77	0.00-0.05		$467 \pm 10^{+9}_{-28}$	$467 \pm 10^{+9}_{-28}$
	0.05-0.10	$250 \pm 30^{+51}_{-32}$	$325 \pm 21^{+42}_{-14}$	$300 \pm 17^{+42}_{-15}$
	0.10-0.15	$234 \pm 30^{+53}_{-6}$	$199 \pm 40^{+33}_{-19}$	$222 \pm 24^{+40}_{-7}$
	0.15-0.20	$108 \pm 35^{+38}_{-31}$		$108 \pm 35^{+38}_{-31}$
	0.20-0.25		$152 \pm 52^{+18}_{-84}$	$152 \pm 52^{+18}_{-84}$
	0.25-0.35		$121 \pm 34^{+9}_{-80}$	$121 \pm 34^{+9}_{-80}$
	0.35-0.50		$8 \pm 4^{+11}_{-1}$	$8 \pm 4^{+11}_{-1}$
0.77-0.80	0.00-0.05		$452 \pm 10^{+10}_{-17}$	$452 \pm 10^{+10}_{-17}$
	0.05-0.10	$248 \pm 39^{+30}_{-27}$	$297 \pm 14^{+13}_{-38}$	$292 \pm 13^{+13}_{-35}$
	0.10-0.15	$196 \pm 23^{+97}_{-7}$	$241 \pm 20^{+50}_{-9}$	$222 \pm 15^{+62}_{-5}$
	0.15-0.20	$198 \pm 48^{+40}_{-39}$	$203 \pm 32^{+97}_{-9}$	$201 \pm 27^{+56}_{-13}$
	0.20-0.25		$168 \pm 54^{+58}_{-46}$	$168 \pm 54^{+58}_{-46}$
0.80-0.83	0.00-0.05		$451 \pm 10^{+9}_{-19}$	$451 \pm 10^{+9}_{-19}$
	0.05-0.10	$353 \pm 74^{+16}_{-117}$	$266 \pm 11^{+18}_{-8}$	$268 \pm 11^{+18}_{-9}$
	0.10-0.15	$197 \pm 25^{+33}_{-14}$	$210 \pm 14^{+7}_{-16}$	$207 \pm 12^{+5}_{-13}$
	0.15-0.20	$84 \pm 23^{+25}_{-13}$	$178 \pm 17^{+5}_{-75}$	$147 \pm 14^{+9}_{-33}$
	0.20-0.25	$73 \pm 32^{+68}_{-52}$	$136 \pm 16^{+9}_{-33}$	$123 \pm 15^{+22}_{-45}$

Table 1 (cont.)

x_L range	p_T^2 range (GeV^2)	$d^2\sigma_{\mathrm{LP}}/dx_L dp_T^2$ s123 ($\mathrm{nb}/\mathrm{GeV}^2$)	$d^2\sigma_{\mathrm{LP}}/dx_L dp_T^2$ s456 ($\mathrm{nb}/\mathrm{GeV}^2$)	$d^2\sigma_{\mathrm{LP}}/dx_L dp_T^2$ Combined ($\mathrm{nb}/\mathrm{GeV}^2$)
	0.25-0.35		$98 \pm 14^{+22}_{-7}$	$98 \pm 14^{+22}_{-7}$
0.83-0.86	0.00-0.05		$434 \pm 10^{+13}_{-19}$	$434 \pm 10^{+13}_{-19}$
	0.05-0.10		$295 \pm 12^{+8}_{-33}$	$295 \pm 12^{+8}_{-33}$
	0.10-0.15	$184 \pm 24^{+79}_{-10}$	$207 \pm 13^{+20}_{-13}$	$202 \pm 11^{+17}_{-5}$
	0.15-0.20	$190 \pm 37^{+33}_{-59}$	$169 \pm 15^{+5}_{-39}$	$172 \pm 14^{+5}_{-39}$
	0.20-0.25	$50 \pm 20^{+22}_{-21}$	$127 \pm 14^{+33}_{-7}$	$102 \pm 11^{+30}_{-19}$
	0.25-0.35		$122 \pm 14^{+7}_{-36}$	$122 \pm 14^{+7}_{-36}$
	0.35-0.50		$49 \pm 8^{+12}_{-6}$	$49 \pm 8^{+12}_{-6}$
0.86-0.89	0.00-0.05		$467 \pm 13^{+24}_{-18}$	$467 \pm 13^{+24}_{-18}$
	0.05-0.10		$309 \pm 12^{+22}_{-20}$	$309 \pm 12^{+22}_{-20}$
	0.10-0.15	$247 \pm 36^{+44}_{-29}$	$232 \pm 14^{+8}_{-20}$	$234 \pm 13^{+7}_{-19}$
	0.15-0.20	$196 \pm 32^{+23}_{-43}$	$180 \pm 15^{+6}_{-35}$	$183 \pm 14^{+6}_{-36}$
	0.20-0.25	$115 \pm 34^{+55}_{-24}$	$136 \pm 14^{+21}_{-16}$	$133 \pm 13^{+20}_{-16}$
	0.25-0.35	$24 \pm 16^{+8}_{-4}$	$81 \pm 8^{+15}_{-11}$	$69 \pm 7^{+24}_{-6}$
	0.35-0.50		$43 \pm 6^{+8}_{-5}$	$43 \pm 6^{+8}_{-5}$
0.89-0.92	0.00-0.05		$481 \pm 19^{+24}_{-19}$	$481 \pm 19^{+24}_{-19}$
	0.05-0.10		$315 \pm 13^{+16}_{-10}$	$315 \pm 13^{+16}_{-10}$
	0.10-0.15	$262 \pm 47^{+68}_{-78}$	$228 \pm 14^{+18}_{-21}$	$231 \pm 13^{+15}_{-24}$
	0.15-0.20	$172 \pm 27^{+28}_{-44}$	$175 \pm 14^{+22}_{-10}$	$174 \pm 12^{+14}_{-11}$
	0.20-0.25	$97 \pm 27^{+58}_{-18}$	$133 \pm 13^{+18}_{-19}$	$126 \pm 12^{+15}_{-11}$
	0.25-0.35	$37 \pm 19^{+18}_{-11}$	$69 \pm 7^{+7}_{-5}$	$65 \pm 6^{+6}_{-5}$
	0.35-0.50		$39 \pm 5^{+6}_{-5}$	$39 \pm 5^{+6}_{-5}$
0.92-0.95	0.00-0.05		$820 \pm 145^{+124}_{-432}$	$820 \pm 145^{+124}_{-432}$
	0.05-0.10		$235 \pm 14^{+54}_{-8}$	$235 \pm 14^{+54}_{-8}$
	0.10-0.15	$221 \pm 58^{+212}_{-36}$	$182 \pm 14^{+48}_{-22}$	$184 \pm 13^{+45}_{-21}$
	0.15-0.20	$138 \pm 21^{+47}_{-11}$	$156 \pm 14^{+33}_{-13}$	$150 \pm 12^{+30}_{-9}$
	0.20-0.25	$92 \pm 22^{+38}_{-10}$	$114 \pm 13^{+17}_{-20}$	$109 \pm 11^{+15}_{-11}$
	0.25-0.35	$39 \pm 15^{+9}_{-18}$	$83 \pm 9^{+16}_{-12}$	$72 \pm 8^{+6}_{-13}$
	0.35-0.50		$36 \pm 5^{+16}_{-4}$	$36 \pm 5^{+16}_{-4}$
0.95-0.98	0.05-0.10		$423 \pm 35^{+63}_{-116}$	$423 \pm 35^{+63}_{-116}$
	0.10-0.15		$328 \pm 30^{+84}_{-10}$	$328 \pm 30^{+84}_{-10}$
	0.15-0.20	$280 \pm 39^{+57}_{-16}$	$250 \pm 32^{+142}_{-5}$	$262 \pm 25^{+90}_{-1}$
	0.20-0.25	$254 \pm 46^{+5}_{-116}$	$197 \pm 32^{+60}_{-6}$	$215 \pm 26^{+30}_{-26}$
	0.25-0.35	$50 \pm 17^{+18}_{-30}$	$190 \pm 34^{+60}_{-72}$	$77 \pm 15^{+19}_{-44}$

Table 1 (cont.)

x_L range	p_T^2 range (GeV^2)	$d^2\sigma_{\rm LP}/dx_L dp_T^2$ s123 (nb/GeV^2)	$d^2\sigma_{\rm LP}/dx_L dp_T^2$ s456 (nb/GeV^2)	$d^2\sigma_{\rm LP}/dx_L dp_T^2$ Combined (nb/GeV^2)
0.98-1.00	0.05-0.10		$2788 \pm 180^{+466}_{-304}$	$2788 \pm 180^{+466}_{-304}$
	0.10-0.15		$1423 \pm 90^{+188}_{-131}$	$1423 \pm 90^{+188}_{-131}$
	0.15-0.20	$1218 \pm 160^{+182}_{-214}$	$1012 \pm 89^{+132}_{-133}$	$1061 \pm 78^{+85}_{-118}$
	0.20-0.25	$574 \pm 81^{+166}_{-35}$	$848 \pm 93^{+186}_{-41}$	$693 \pm 61^{+174}_{-16}$
	0.25-0.35	$231 \pm 54^{+116}_{-13}$	$588 \pm 69^{+39}_{-93}$	$367 \pm 42^{+147}_{-26}$

x_L range	b (GeV^{-2})
0.50 - 0.56	$6.98^{+1.11+2.99}_{-1.06-1.53}$
0.56 - 0.62	$8.49^{+0.47+2.18}_{-0.51-1.32}$
0.62 - 0.65	$7.36^{+0.34+1.12}_{-0.38-0.54}$
0.65 - 0.68	$6.83^{+0.26+0.78}_{-0.26-0.38}$
0.68 - 0.71	$7.01^{+0.21+0.15}_{-0.21-0.51}$
0.71 - 0.74	$7.43^{+0.26+0.63}_{-0.26-0.38}$
0.74 - 0.77	$7.48^{+0.38+1.23}_{-0.38-1.00}$
0.77 - 0.80	$6.82^{+0.30+0.90}_{-0.34-1.24}$
0.80 - 0.83	$6.54^{+0.21+0.52}_{-0.21-0.40}$
0.83 - 0.86	$5.88^{+0.17+0.75}_{-0.17-0.18}$
0.86 - 0.89	$6.82^{+0.17+0.82}_{-0.17-0.64}$
0.89 - 0.92	$7.22^{+0.21+0.72}_{-0.21-0.75}$
0.92 - 0.95	$6.00^{+0.26+0.48}_{-0.26-1.37}$
0.95 - 0.98	$4.45^{+0.47+1.69}_{-0.47-0.88}$
0.98 - 1.00	$8.31^{+0.34+1.05}_{-0.38-0.91}$

Table 2: *The p_T^2-slope, b, of the cross section $d^2\sigma_{\rm LP}/dx_L dp_T^2$ as obtained by a fit to the data of a function $A \cdot e^{-b \cdot p_T^2}$ in bins of x_L. Statistical uncertainties are listed first, followed by systematic uncertainties.*

x_L range	b (GeV^{-2})	
	$\langle Q^2 \rangle = 5.1$ GeV^2	$\langle Q^2 \rangle = 30.6$ GeV^2
0.5 - 0.65	$6.90^{+0.38+1.34}_{-0.43-0.18}$	$7.97^{+0.43+1.06}_{-0.38-0.39}$
0.65 - 0.8	$7.00^{+0.17+0.20}_{-0.17-0.21}$	$7.13^{+0.17+0.16}_{-0.17-0.31}$
0.8 - 0.92	$7.29^{+0.13+0.15}_{-0.17-0.49}$	$6.10^{+0.13+0.64}_{-0.13-0.04}$
0.92 - 1.0	$6.74^{+0.26+0.28}_{-0.30-0.33}$	$6.06^{+0.30+0.66}_{-0.30-0.36}$

Table 3: *The p_T^2-slope, b, of the cross section $d^2\sigma_{\rm LP}/dx_L dp_T^2$ as obtained by a fit to the data of a function $A \cdot e^{-b \cdot p_T^2}$ in bins of x_L, measured in two ranges of Q^2. Statistical uncertainties are listed first, followed by systematic uncertainties.*

x_L range	$1/\sigma_{\rm tot} \cdot d\sigma_{\rm LP}/dx_L$		
	$0 < p_T^2 < 0.04$ GeV^2	$0.04 < p_T^2 < 0.15$ GeV^2	$0.15 < p_T^2 < 0.5$ GeV^2
0.32 - 0.38	$0.091 \pm 0.008^{+0.009}_{-0.013}$		
0.38 - 0.44	$0.082 \pm 0.004^{+0.005}_{-0.008}$	$0.156 \pm 0.016^{+0.013}_{-0.024}$	
0.44 - 0.50	$0.086 \pm 0.004^{+0.003}_{-0.010}$	$0.144 \pm 0.013^{+0.005}_{-0.021}$	
0.50 - 0.56	$0.091 \pm 0.004^{+0.004}_{-0.006}$	$0.140 \pm 0.006^{+0.026}_{-0.008}$	
0.56 - 0.62	$0.097 \pm 0.004^{+0.002}_{-0.010}$	$0.143 \pm 0.004^{+0.004}_{-0.014}$	
0.62 - 0.68	$0.096 \pm 0.003^{+0.003}_{-0.005}$	$0.142 \pm 0.005^{+0.002}_{-0.021}$	$0.126 \pm 0.007^{+0.010}_{-0.011}$
0.68 - 0.74	$0.100 \pm 0.002^{+0.003}_{-0.005}$	$0.141 \pm 0.005^{+0.004}_{-0.012}$	$0.138 \pm 0.008^{+0.008}_{-0.009}$
0.74 - 0.80	$0.094 \pm 0.001^{+0.000}_{-0.007}$	$0.145 \pm 0.003^{+0.003}_{-0.006}$	$0.155 \pm 0.015^{+0.010}_{-0.015}$
0.80 - 0.86	$0.091 \pm 0.001^{+0.001}_{-0.005}$	$0.139 \pm 0.003^{+0.001}_{-0.008}$	$0.146 \pm 0.005^{+0.010}_{-0.023}$
0.86 - 0.92	$0.099 \pm 0.002^{+0.002}_{-0.007}$	$0.154 \pm 0.003^{+0.005}_{-0.007}$	$0.143 \pm 0.004^{+0.011}_{-0.014}$
0.92 - 0.98		$0.167 \pm 0.006^{+0.020}_{-0.015}$	$0.179 \pm 0.007^{+0.021}_{-0.013}$
0.97 - 1.00		$1.126 \pm 0.047^{+0.113}_{-0.092}$	$0.816 \pm 0.036^{+0.088}_{-0.055}$

Table 4: *The leading-proton production rate $1/\sigma_{\rm tot} \cdot d\sigma_{\rm LP}/dx_L$ as a function of x_L measured in three ranges of p_T^2. Statistical uncertainties are listed first, followed by systematic uncertainties.*

x_L range	$1/\sigma_{\rm tot} \cdot d\sigma_{\rm LP}/dx_L$
0.32 - 0.38	$0.372 \pm 0.026^{+0.046}_{-0.062}$
0.38 - 0.44	$0.309 \pm 0.018^{+0.037}_{-0.037}$
0.44 - 0.50	$0.339 \pm 0.012^{+0.033}_{-0.044}$
0.50 - 0.56	$0.358 \pm 0.010^{+0.047}_{-0.030}$
0.56 - 0.62	$0.371 \pm 0.009^{+0.029}_{-0.039}$
0.62 - 0.65	$0.371 \pm 0.011^{+0.025}_{-0.037}$
0.65 - 0.68	$0.385 \pm 0.010^{+0.027}_{-0.031}$
0.68 - 0.71	$0.418 \pm 0.010^{+0.030}_{-0.037}$
0.71 - 0.74	$0.398 \pm 0.009^{+0.039}_{-0.036}$
0.74 - 0.77	$0.408 \pm 0.008^{+0.038}_{-0.039}$
0.77 - 0.80	$0.398 \pm 0.007^{+0.036}_{-0.037}$
0.80 - 0.83	$0.376 \pm 0.006^{+0.029}_{-0.035}$
0.83 - 0.86	$0.382 \pm 0.006^{+0.026}_{-0.033}$
0.86 - 0.89	$0.405 \pm 0.007^{+0.024}_{-0.030}$
0.89 - 0.92	$0.395 \pm 0.008^{+0.019}_{-0.026}$
0.92 - 0.95	$0.325 \pm 0.010^{+0.044}_{-0.016}$
0.95 - 0.98	$0.562 \pm 0.023^{+0.058}_{-0.049}$
0.98 - 1.00	$2.478 \pm 0.076^{+0.235}_{-0.136}$

Table 5: *The leading-proton production rate $1/\sigma_{\rm tot} \cdot d\sigma_{\rm LP}/dx_L$ as a function of x_L measured in the region $p_T^2 < 0.5$ GeV^2. Statistical uncertainties are listed first, followed by systematic uncertainties.*

$\langle x \rangle$	$\langle Q^2 \rangle$ (GeV^2)	x_L range	$r^{\mathrm{LP}(3)}$
$9.6 \cdot 10^{-5}$	4.2	0.32 - 0.42	$0.365 \pm 0.086^{+0.066}_{-0.168}$
		0.42 - 0.52	$0.268 \pm 0.040^{+0.085}_{-0.041}$
		0.52 - 0.62	$0.391 \pm 0.041^{+0.050}_{-0.048}$
		0.62 - 0.72	$0.338 \pm 0.026^{+0.058}_{-0.025}$
		0.72 - 0.72	$0.378 \pm 0.024^{+0.050}_{-0.049}$
		0.82 - 0.72	$0.458 \pm 0.027^{+0.032}_{-0.076}$
$1.7 \cdot 10^{-4}$	4.2	0.32 - 0.42	$0.414 \pm 0.063^{+0.050}_{-0.135}$
		0.42 - 0.52	$0.310 \pm 0.032^{+0.039}_{-0.029}$
		0.52 - 0.62	$0.370 \pm 0.026^{+0.037}_{-0.036}$
		0.62 - 0.72	$0.366 \pm 0.019^{+0.028}_{-0.035}$
		0.72 - 0.82	$0.390 \pm 0.015^{+0.039}_{-0.034}$
		0.82 - 0.92	$0.378 \pm 0.014^{+0.026}_{-0.036}$
$3.5 \cdot 10^{-4}$	4.2	0.32 - 0.42	$0.351 \pm 0.061^{+0.047}_{-0.062}$
		0.42 - 0.52	$0.269 \pm 0.029^{+0.055}_{-0.028}$
		0.52 - 0.62	$0.354 \pm 0.025^{+0.067}_{-0.029}$
		0.62 - 0.72	$0.406 \pm 0.022^{+0.030}_{-0.063}$
		0.72 - 0.82	$0.405 \pm 0.017^{+0.040}_{-0.038}$
		0.82 - 0.92	$0.364 \pm 0.014^{+0.023}_{-0.029}$
$6.9 \cdot 10^{-4}$	4.2	0.32 - 0.42	$0.275 \pm 0.057^{+0.063}_{-0.047}$
		0.42 - 0.52	$0.308 \pm 0.035^{+0.038}_{-0.031}$
		0.52 - 0.62	$0.339 \pm 0.027^{+0.045}_{-0.034}$
		0.62 - 0.72	$0.326 \pm 0.020^{+0.026}_{-0.027}$
		0.72 - 0.82	$0.400 \pm 0.018^{+0.063}_{-0.031}$
		0.82 - 0.92	$0.403 \pm 0.017^{+0.030}_{-0.070}$
$1.46 \cdot 10^{-3}$	4.2	0.32 - 0.42	$0.272 \pm 0.083^{+0.040}_{-0.082}$
		0.42 - 0.52	$0.268 \pm 0.045^{+0.066}_{-0.035}$
		0.52 - 0.62	$0.285 \pm 0.038^{+0.047}_{-0.039}$
		0.62 - 0.72	$0.355 \pm 0.029^{+0.041}_{-0.023}$
		0.72 - 0.82	$0.362 \pm 0.022^{+0.057}_{-0.046}$
		0.82 - 0.92	$0.359 \pm 0.021^{+0.025}_{-0.034}$

Table 6: *The leading-proton production rate $r^{\mathrm{LP}(3)}$ measured as a function of x_L for protons with $p_T^2 < 0.5$ GeV^2, in bins of x and Q^2, with averages $\langle x \rangle$ and $\langle Q^2 \rangle$. Statistical uncertainties are listed first, followed by systematic uncertainties.*

Table 6 (cont.)

$\langle x \rangle$	$\langle Q^2 \rangle$ (GeV^2)	x_L range	$r^{\mathrm{LP}(3)}$
$1.9 \cdot 10^{-4}$	7.3	0.32 - 0.42	$0.314 \pm 0.084^{+0.087}_{-0.055}$
		0.42 - 0.52	$0.430 \pm 0.061^{+0.065}_{-0.122}$
		0.52 - 0.62	$0.299 \pm 0.031^{+0.049}_{-0.027}$
		0.62 - 0.72	$0.355 \pm 0.027^{+0.041}_{-0.029}$
		0.72 - 0.82	$0.382 \pm 0.024^{+0.039}_{-0.042}$
		0.82 - 0.92	$0.383 \pm 0.022^{+0.028}_{-0.083}$
$3.4 \cdot 10^{-4}$	7.3	0.32 - 0.42	$0.340 \pm 0.076^{+0.062}_{-0.075}$
		0.42 - 0.52	$0.360 \pm 0.044^{+0.040}_{-0.062}$
		0.52 - 0.62	$0.369 \pm 0.032^{+0.044}_{-0.029}$
		0.62 - 0.72	$0.347 \pm 0.022^{+0.030}_{-0.038}$
		0.72 - 0.82	$0.374 \pm 0.019^{+0.037}_{-0.033}$
		0.82 - 0.92	$0.359 \pm 0.016^{+0.037}_{-0.020}$
$6.9 \cdot 10^{-4}$	7.3	0.32 - 0.42	$0.392 \pm 0.081^{+0.056}_{-0.102}$
		0.42 - 0.52	$0.261 \pm 0.038^{+0.029}_{-0.086}$
		0.52 - 0.62	$0.372 \pm 0.034^{+0.048}_{-0.028}$
		0.62 - 0.72	$0.363 \pm 0.025^{+0.028}_{-0.047}$
		0.72 - 0.82	$0.385 \pm 0.020^{+0.034}_{-0.040}$
		0.82 - 0.92	$0.388 \pm 0.019^{+0.027}_{-0.037}$
$1.36 \cdot 10^{-3}$	7.3	0.32 - 0.42	$0.275 \pm 0.062^{+0.106}_{-0.061}$
		0.42 - 0.52	$0.401 \pm 0.056^{+0.050}_{-0.088}$
		0.52 - 0.62	$0.393 \pm 0.039^{+0.043}_{-0.035}$
		0.62 - 0.72	$0.448 \pm 0.032^{+0.042}_{-0.057}$
		0.72 - 0.82	$0.394 \pm 0.021^{+0.042}_{-0.043}$
		0.82 - 0.92	$0.389 \pm 0.020^{+0.033}_{-0.025}$
$2.67 \cdot 10^{-3}$	7.3	0.32 - 0.47	$0.290 \pm 0.097^{+0.034}_{-0.112}$
		0.47 - 0.62	$0.442 \pm 0.086^{+0.092}_{-0.159}$
		0.62 - 0.77	$0.449 \pm 0.050^{+0.094}_{-0.046}$
		0.77 - 0.92	$0.398 \pm 0.033^{+0.049}_{-0.054}$
$2.6 \cdot 10^{-4}$	11	0.32 - 0.47	$0.349 \pm 0.078^{+0.042}_{-0.128}$
		0.47 - 0.62	$0.285 \pm 0.034^{+0.111}_{-0.023}$
		0.62 - 0.77	$0.485 \pm 0.037^{+0.041}_{-0.074}$
		0.77 - 0.92	$0.371 \pm 0.021^{+0.033}_{-0.024}$

Table 6 (cont.)

$\langle x \rangle$	$\langle Q^2 \rangle$ (GeV^2)	x_L range	$r^{\mathrm{LP}(3)}$
$4.6 \cdot 10^{-4}$	11	0.32 - 0.42	$0.482 \pm 0.097^{+0.067}_{-0.162}$
		0.42 - 0.52	$0.285 \pm 0.036^{+0.037}_{-0.039}$
		0.52 - 0.62	$0.370 \pm 0.031^{+0.064}_{-0.033}$
		0.62 - 0.72	$0.435 \pm 0.028^{+0.034}_{-0.054}$
		0.72 - 0.82	$0.386 \pm 0.019^{+0.051}_{-0.030}$
		0.82 - 0.92	$0.365 \pm 0.016^{+0.049}_{-0.018}$
$9.2 \cdot 10^{-4}$	11	0.32 - 0.42	$0.418 \pm 0.084^{+0.056}_{-0.093}$
		0.42 - 0.52	$0.286 \pm 0.037^{+0.064}_{-0.028}$
		0.52 - 0.62	$0.408 \pm 0.034^{+0.041}_{-0.035}$
		0.62 - 0.72	$0.392 \pm 0.024^{+0.052}_{-0.027}$
		0.72 - 0.82	$0.392 \pm 0.019^{+0.039}_{-0.056}$
		0.82 - 0.92	$0.397 \pm 0.018^{+0.024}_{-0.044}$
$1.83 \cdot 10^{-3}$	11	0.32 - 0.42	$0.361 \pm 0.075^{+0.058}_{-0.056}$
		0.42 - 0.52	$0.353 \pm 0.047^{+0.039}_{-0.077}$
		0.52 - 0.62	$0.375 \pm 0.033^{+0.036}_{-0.073}$
		0.62 - 0.72	$0.411 \pm 0.026^{+0.030}_{-0.027}$
		0.72 - 0.82	$0.348 \pm 0.017^{+0.043}_{-0.026}$
		0.82 - 0.92	$0.378 \pm 0.017^{+0.051}_{-0.021}$
$3.98 \cdot 10^{-3}$	11	0.32 - 0.47	$0.228 \pm 0.063^{+0.033}_{-0.090}$
		0.47 - 0.62	$0.378 \pm 0.047^{+0.043}_{-0.063}$
		0.62 - 0.77	$0.421 \pm 0.033^{+0.034}_{-0.105}$
		0.77 - 0.92	$0.448 \pm 0.026^{+0.038}_{-0.057}$
$5.1 \cdot 10^{-4}$	22	0.32 - 0.47	$0.470 \pm 0.111^{+0.061}_{-0.281}$
		0.47 - 0.62	$0.306 \pm 0.037^{+0.045}_{-0.028}$
		0.62 - 0.77	$0.436 \pm 0.035^{+0.044}_{-0.043}$
		0.77 - 0.92	$0.388 \pm 0.023^{+0.042}_{-0.027}$
$9.2 \cdot 10^{-4}$	22	0.32 - 0.42	$0.356 \pm 0.084^{+0.137}_{-0.071}$
		0.42 - 0.52	$0.350 \pm 0.053^{+0.044}_{-0.044}$
		0.52 - 0.62	$0.376 \pm 0.039^{+0.058}_{-0.030}$
		0.62 - 0.72	$0.401 \pm 0.030^{+0.031}_{-0.057}$
		0.72 - 0.82	$0.386 \pm 0.022^{+0.056}_{-0.029}$
		0.82 - 0.92	$0.411 \pm 0.022^{+0.026}_{-0.041}$
$1.84 \cdot 10^{-3}$	22	0.32 - 0.42	$0.367 \pm 0.084^{+0.091}_{-0.075}$
		0.42 - 0.52	$0.241 \pm 0.038^{+0.075}_{-0.024}$

Table 6 (cont.)

$\langle x \rangle$	$\langle Q^2 \rangle$ (GeV^2)	x_L range	$r^{\mathrm{LP}(3)}$
		0.52 - 0.62	$0.347 \pm 0.034^{+0.055}_{-0.033}$
		0.62 - 0.72	$0.353 \pm 0.025^{+0.060}_{-0.027}$
		0.72 - 0.82	$0.378 \pm 0.021^{+0.036}_{-0.035}$
		0.82 - 0.92	$0.401 \pm 0.021^{+0.048}_{-0.026}$
$3.66 \cdot 10^{-3}$	22	0.32 - 0.42	$0.297 \pm 0.078^{+0.145}_{-0.042}$
		0.42 - 0.52	$0.386 \pm 0.066^{+0.078}_{-0.034}$
		0.52 - 0.62	$0.457 \pm 0.055^{+0.066}_{-0.071}$
		0.62 - 0.72	$0.442 \pm 0.038^{+0.035}_{-0.077}$
		0.72 - 0.82	$0.453 \pm 0.029^{+0.059}_{-0.033}$
		0.82 - 0.92	$0.377 \pm 0.023^{+0.027}_{-0.040}$
$7.83 \cdot 10^{-3}$	22	0.32 - 0.47	$0.215 \pm 0.066^{+0.232}_{-0.102}$
		0.47 - 0.62	$0.354 \pm 0.053^{+0.087}_{-0.060}$
		0.62 - 0.77	$0.399 \pm 0.036^{+0.079}_{-0.032}$
		0.77 - 0.92	$0.442 \pm 0.030^{+0.060}_{-0.077}$
$1.03 \cdot 10^{-3}$	44	0.32 - 0.47	$0.356 \pm 0.104^{+0.100}_{-0.062}$
		0.47 - 0.62	$0.327 \pm 0.052^{+0.074}_{-0.039}$
		0.62 - 0.77	$0.373 \pm 0.038^{+0.051}_{-0.034}$
		0.77 - 0.92	$0.381 \pm 0.030^{+0.027}_{-0.030}$
$1.86 \cdot 10^{-3}$	44	0.37 - 0.42	$0.508 \pm 0.150^{+0.221}_{-0.116}$
		0.47 - 0.52	$0.346 \pm 0.073^{+0.049}_{-0.077}$
		0.57 - 0.62	$0.444 \pm 0.063^{+0.043}_{-0.112}$
		0.67 - 0.72	$0.348 \pm 0.041^{+0.027}_{-0.049}$
		0.77 - 0.82	$0.413 \pm 0.033^{+0.044}_{-0.052}$
		0.87 - 0.92	$0.352 \pm 0.026^{+0.051}_{-0.021}$
$3.68 \cdot 10^{-3}$	44	0.37 - 0.42	$0.221 \pm 0.088^{+0.065}_{-0.027}$
		0.47 - 0.52	$0.456 \pm 0.097^{+0.079}_{-0.105}$
		0.57 - 0.62	$0.303 \pm 0.046^{+0.052}_{-0.023}$
		0.67 - 0.72	$0.496 \pm 0.057^{+0.036}_{-0.150}$
		0.77 - 0.82	$0.511 \pm 0.044^{+0.061}_{-0.056}$
		0.87 - 0.92	$0.408 \pm 0.033^{+0.041}_{-0.029}$
$7.33 \cdot 10^{-3}$	44	0.37 - 0.42	$0.628 \pm 0.226^{+0.297}_{-0.190}$
		0.47 - 0.52	$0.341 \pm 0.090^{+0.053}_{-0.060}$
		0.57 - 0.62	$0.418 \pm 0.074^{+0.153}_{-0.035}$
		0.67 - 0.72	$0.458 \pm 0.061^{+0.044}_{-0.070}$

Table 6 (cont.)

$\langle x \rangle$	$\langle Q^2 \rangle$ (GeV^2)	x_L range	$r^{\mathrm{LP}(3)}$
		0.77 - 0.82	$0.501 \pm 0.048^{+0.055}_{-0.081}$
		0.87 - 0.92	$0.448 \pm 0.039^{+0.042}_{-0.030}$
$1.54 \cdot 10^{-2}$	44	0.32 - 0.52	$0.453 \pm 0.135^{+0.078}_{-0.363}$
		0.52 - 0.72	$0.454 \pm 0.062^{+0.048}_{-0.071}$
		0.72 - 0.92	$0.385 \pm 0.033^{+0.083}_{-0.027}$
$2.00 \cdot 10^{-3}$	88	0.32 - 0.47	$0.328 \pm 0.162^{+0.151}_{-0.064}$
		0.47 - 0.62	$0.462 \pm 0.121^{+0.111}_{-0.122}$
		0.62 - 0.77	$0.307 \pm 0.045^{+0.045}_{-0.030}$
		0.77 - 0.92	$0.339 \pm 0.040^{+0.048}_{-0.033}$
$3.59 \cdot 10^{-3}$	88	0.32 - 0.47	$0.449 \pm 0.145^{+0.058}_{-0.134}$
		0.47 - 0.62	$0.509 \pm 0.090^{+0.120}_{-0.098}$
		0.62 - 0.77	$0.402 \pm 0.049^{+0.194}_{-0.034}$
		0.77 - 0.92	$0.393 \pm 0.034^{+0.068}_{-0.022}$
$7.37 \cdot 10^{-3}$	88	0.32 - 0.47	$0.491 \pm 0.178^{+0.164}_{-0.131}$
		0.47 - 0.62	$0.345 \pm 0.078^{+0.050}_{-0.042}$
		0.62 - 0.77	$0.364 \pm 0.046^{+0.028}_{-0.034}$
		0.77 - 0.92	$0.440 \pm 0.042^{+0.087}_{-0.032}$
$1.42 \cdot 10^{-2}$	88	0.32 - 0.47	$0.351 \pm 0.133^{+0.171}_{-0.054}$
		0.47 - 0.62	$0.479 \pm 0.101^{+0.169}_{-0.103}$
		0.62 - 0.77	$0.390 \pm 0.054^{+0.098}_{-0.037}$
		0.77 - 0.92	$0.498 \pm 0.050^{+0.042}_{-0.112}$
$3.01 \cdot 10^{-2}$	88	0.32 - 0.52	$0.449 \pm 0.211^{+0.075}_{-0.264}$
		0.52 - 0.72	$0.330 \pm 0.063^{+0.121}_{-0.023}$
		0.72 - 0.92	$0.440 \pm 0.056^{+0.062}_{-0.044}$
$4.00 \cdot 10^{-3}$	237	0.32 - 0.52	$0.250 \pm 0.153^{+0.115}_{-0.129}$
		0.52 - 0.72	$0.175 \pm 0.068^{+0.241}_{-0.013}$
		0.72 - 0.92	$0.451 \pm 0.071^{+0.079}_{-0.044}$
$7.52 \cdot 10^{-3}$	237	0.32 - 0.52	$0.467 \pm 0.195^{+0.105}_{-0.086}$
		0.52 - 0.72	$0.482 \pm 0.088^{+0.067}_{-0.205}$
		0.72 - 0.92	$0.430 \pm 0.049^{+0.069}_{-0.053}$
$1.47 \cdot 10^{-2}$	237	0.32 - 0.47	$0.301 \pm 0.156^{+0.366}_{-0.040}$
		0.47 - 0.62	$0.249 \pm 0.074^{+0.087}_{-0.037}$
		0.62 - 0.77	$0.445 \pm 0.070^{+0.112}_{-0.040}$
		0.77 - 0.92	$0.381 \pm 0.045^{+0.040}_{-0.028}$

Table 6 (cont.)

$\langle x \rangle$	$\langle Q^2 \rangle$ (GeV^2)	x_L range	$r^{\mathrm{LP}(3)}$
$3.25 \cdot 10^{-2}$	237	0.32 - 0.47	$0.102 \pm 0.082^{+0.119}_{-0.011}$
		0.47 - 0.62	$0.355 \pm 0.090^{+0.049}_{-0.072}$
		0.62 - 0.77	$0.359 \pm 0.055^{+0.135}_{-0.028}$
		0.77 - 0.92	$0.403 \pm 0.049^{+0.041}_{-0.064}$

$\langle x \rangle$	$\langle Q^2 \rangle$ (GeV^2)	x_L range	$r^{\mathrm{LP}(3)}$
$9.6 \cdot 10^{-5}$	4.2	0.32 - 0.47	$0.082 \pm 0.015^{+0.043}_{-0.014}$
		0.47 - 0.62	$0.091 \pm 0.012^{+0.015}_{-0.019}$
		0.62 - 0.77	$0.080 \pm 0.006^{+0.005}_{-0.026}$
		0.77 - 0.92	$0.104 \pm 0.008^{+0.007}_{-0.014}$
$1.7 \cdot 10^{-4}$	4.2	0.32 - 0.47	$0.103 \pm 0.013^{+0.006}_{-0.026}$
		0.47 - 0.62	$0.083 \pm 0.008^{+0.009}_{-0.010}$
		0.62 - 0.77	$0.096 \pm 0.005^{+0.003}_{-0.023}$
		0.77 - 0.92	$0.089 \pm 0.004^{+0.003}_{-0.008}$
$3.5 \cdot 10^{-4}$	4.2	0.32 - 0.47	$0.077 \pm 0.010^{+0.009}_{-0.009}$
		0.47 - 0.62	$0.087 \pm 0.008^{+0.012}_{-0.006}$
		0.62 - 0.77	$0.108 \pm 0.006^{+0.009}_{-0.007}$
		0.77 - 0.92	$0.093 \pm 0.004^{+0.004}_{-0.003}$
$6.9 \cdot 10^{-4}$	4.2	0.32 - 0.47	$0.077 \pm 0.012^{+0.013}_{-0.004}$
		0.47 - 0.62	$0.085 \pm 0.009^{+0.007}_{-0.007}$
		0.62 - 0.77	$0.095 \pm 0.006^{+0.009}_{-0.002}$
		0.77 - 0.92	$0.087 \pm 0.004^{+0.006}_{-0.002}$
$1.46 \cdot 10^{-3}$	4.2	0.32 - 0.47	$0.074 \pm 0.016^{+0.012}_{-0.015}$
		0.47 - 0.62	$0.046 \pm 0.008^{+0.011}_{-0.004}$
		0.62 - 0.77	$0.083 \pm 0.006^{+0.012}_{-0.003}$
		0.77 - 0.92	$0.086 \pm 0.006^{+0.005}_{-0.007}$

Table 7: *The leading-proton production rate $r^{\mathrm{LP}(3)}$ measured as a function of x_L for protons with $p_T^2 < 0.04$ GeV^2, in bins of x and Q^2, with averages $\langle x \rangle$ and $\langle Q^2 \rangle$. Statistical uncertainties are listed first, followed by systematic uncertainties.*

Table 7 (cont.)

$\langle x \rangle$	$\langle Q^2 \rangle$ (GeV^2)	x_L range	$r^{\mathrm{LP}(3)}$
$1.9 \cdot 10^{-4}$	7.3	0.32 - 0.47	$0.093 \pm 0.017^{+0.009}_{-0.015}$
		0.47 - 0.62	$0.098 \pm 0.012^{+0.008}_{-0.027}$
		0.62 - 0.77	$0.087 \pm 0.007^{+0.013}_{-0.003}$
		0.77 - 0.92	$0.092 \pm 0.007^{+0.006}_{-0.015}$
$3.4 \cdot 10^{-4}$	7.3	0.32 - 0.47	$0.090 \pm 0.015^{+0.012}_{-0.019}$
		0.47 - 0.62	$0.103 \pm 0.011^{+0.006}_{-0.011}$
		0.62 - 0.77	$0.079 \pm 0.005^{+0.007}_{-0.002}$
		0.77 - 0.92	$0.088 \pm 0.005^{+0.004}_{-0.003}$
$6.9 \cdot 10^{-4}$	7.3	0.32 - 0.47	$0.090 \pm 0.015^{+0.005}_{-0.025}$
		0.47 - 0.62	$0.093 \pm 0.011^{+0.004}_{-0.017}$
		0.62 - 0.77	$0.102 \pm 0.007^{+0.004}_{-0.006}$
		0.77 - 0.92	$0.095 \pm 0.006^{+0.002}_{-0.017}$
$1.36 \cdot 10^{-3}$	7.3	0.32 - 0.47	$0.075 \pm 0.014^{+0.011}_{-0.006}$
		0.47 - 0.62	$0.104 \pm 0.013^{+0.010}_{-0.014}$
		0.62 - 0.77	$0.113 \pm 0.008^{+0.003}_{-0.017}$
		0.77 - 0.92	$0.098 \pm 0.006^{+0.006}_{-0.009}$
$2.67 \cdot 10^{-3}$	7.3	0.32 - 0.47	$0.067 \pm 0.025^{+0.007}_{-0.034}$
		0.47 - 0.62	$0.112 \pm 0.028^{+0.023}_{-0.036}$
		0.62 - 0.77	$0.097 \pm 0.015^{+0.017}_{-0.012}$
		0.77 - 0.92	$0.095 \pm 0.011^{+0.003}_{-0.017}$
$2.6 \cdot 10^{-4}$	11	0.32 - 0.47	$0.098 \pm 0.024^{+0.006}_{-0.031}$
		0.47 - 0.62	$0.075 \pm 0.013^{+0.038}_{-0.006}$
		0.62 - 0.77	$0.129 \pm 0.014^{+0.005}_{-0.011}$
		0.77 - 0.92	$0.085 \pm 0.008^{+0.003}_{-0.005}$
$4.6 \cdot 10^{-4}$	11	0.32 - 0.47	$0.114 \pm 0.018^{+0.008}_{-0.027}$
		0.47 - 0.62	$0.081 \pm 0.009^{+0.014}_{-0.004}$
		0.62 - 0.77	$0.101 \pm 0.007^{+0.003}_{-0.011}$
		0.77 - 0.92	$0.099 \pm 0.006^{+0.007}_{-0.003}$
$9.2 \cdot 10^{-4}$	11	0.32 - 0.47	$0.080 \pm 0.013^{+0.009}_{-0.006}$
		0.47 - 0.62	$0.110 \pm 0.012^{+0.019}_{-0.004}$
		0.62 - 0.77	$0.080 \pm 0.006^{+0.009}_{-0.007}$
		0.77 - 0.92	$0.091 \pm 0.005^{+0.002}_{-0.005}$

Table 7 (cont.)

$\langle x \rangle$	$\langle Q^2 \rangle$ (GeV^2)	x_L range	$r^{\mathrm{LP}(3)}$
$1.83 \cdot 10^{-3}$	11	0.32 - 0.47	$0.082 \pm 0.015^{+0.008}_{-0.007}$
		0.47 - 0.62	$0.094 \pm 0.011^{+0.004}_{-0.018}$
		0.62 - 0.77	$0.100 \pm 0.007^{+0.004}_{-0.006}$
		0.77 - 0.92	$0.089 \pm 0.005^{+0.008}_{-0.002}$
$3.98 \cdot 10^{-3}$	11	0.32 - 0.47	$0.041 \pm 0.015^{+0.009}_{-0.020}$
		0.47 - 0.62	$0.118 \pm 0.021^{+0.010}_{-0.042}$
		0.62 - 0.77	$0.102 \pm 0.010^{+0.003}_{-0.024}$
		0.77 - 0.92	$0.107 \pm 0.009^{+0.006}_{-0.014}$
$5.1 \cdot 10^{-4}$	22	0.32 - 0.47	$0.098 \pm 0.029^{+0.013}_{-0.056}$
		0.47 - 0.62	$0.081 \pm 0.014^{+0.010}_{-0.006}$
		0.62 - 0.77	$0.114 \pm 0.014^{+0.021}_{-0.007}$
		0.77 - 0.92	$0.088 \pm 0.009^{+0.005}_{-0.023}$
$9.2 \cdot 10^{-4}$	22	0.32 - 0.47	$0.094 \pm 0.018^{+0.007}_{-0.020}$
		0.47 - 0.62	$0.094 \pm 0.012^{+0.018}_{-0.003}$
		0.62 - 0.77	$0.100 \pm 0.008^{+0.009}_{-0.008}$
		0.77 - 0.92	$0.090 \pm 0.006^{+0.008}_{-0.004}$
$1.84 \cdot 10^{-3}$	22	0.32 - 0.47	$0.089 \pm 0.017^{+0.022}_{-0.008}$
		0.47 - 0.62	$0.080 \pm 0.010^{+0.007}_{-0.010}$
		0.62 - 0.77	$0.089 \pm 0.007^{+0.003}_{-0.007}$
		0.77 - 0.92	$0.089 \pm 0.006^{+0.010}_{-0.004}$
$3.66 \cdot 10^{-3}$	22	0.32 - 0.47	$0.078 \pm 0.017^{+0.026}_{-0.005}$
		0.47 - 0.62	$0.120 \pm 0.019^{+0.009}_{-0.028}$
		0.62 - 0.77	$0.114 \pm 0.010^{+0.007}_{-0.010}$
		0.77 - 0.92	$0.099 \pm 0.007^{+0.013}_{-0.002}$
$7.83 \cdot 10^{-3}$	22	0.32 - 0.47	$0.054 \pm 0.019^{+0.050}_{-0.024}$
		0.47 - 0.62	$0.087 \pm 0.018^{+0.011}_{-0.043}$
		0.62 - 0.77	$0.087 \pm 0.010^{+0.041}_{-0.005}$
		0.77 - 0.92	$0.116 \pm 0.012^{+0.033}_{-0.016}$
$1.03 \cdot 10^{-3}$	44	0.32 - 0.47	$0.092 \pm 0.031^{+0.020}_{-0.017}$
		0.47 - 0.62	$0.086 \pm 0.020^{+0.048}_{-0.010}$
		0.62 - 0.77	$0.105 \pm 0.016^{+0.018}_{-0.031}$
		0.77 - 0.92	$0.108 \pm 0.013^{+0.015}_{-0.005}$
$1.86 \cdot 10^{-3}$	44	0.32 - 0.47	$0.096 \pm 0.023^{+0.024}_{-0.010}$
		0.47 - 0.62	$0.087 \pm 0.016^{+0.005}_{-0.028}$

Table 7 (cont.)

$\langle x \rangle$	$\langle Q^2 \rangle$ (GeV^2)	x_L range	$r^{\mathrm{LP}(3)}$
		0.62 - 0.77	$0.130 \pm 0.015^{+0.004}_{-0.029}$
		0.77 - 0.92	$0.102 \pm 0.010^{+0.004}_{-0.016}$
$3.68 \cdot 10^{-3}$	44	0.32 - 0.47	$0.077 \pm 0.023^{+0.038}_{-0.011}$
		0.47 - 0.62	$0.079 \pm 0.016^{+0.004}_{-0.019}$
		0.62 - 0.77	$0.139 \pm 0.017^{+0.005}_{-0.023}$
		0.77 - 0.92	$0.117 \pm 0.012^{+0.003}_{-0.013}$
$7.33 \cdot 10^{-3}$	44	0.32 - 0.47	$0.124 \pm 0.039^{+0.021}_{-0.030}$
		0.47 - 0.62	$0.104 \pm 0.023^{+0.027}_{-0.005}$
		0.62 - 0.77	$0.107 \pm 0.015^{+0.022}_{-0.004}$
		0.77 - 0.92	$0.096 \pm 0.011^{+0.023}_{-0.004}$
$1.54 \cdot 10^{-2}$	44	0.32 - 0.47	$0.076 \pm 0.036^{+0.075}_{-0.017}$
		0.47 - 0.62	$0.118 \pm 0.034^{+0.020}_{-0.040}$
		0.62 - 0.77	$0.108 \pm 0.019^{+0.036}_{-0.009}$
		0.77 - 0.92	$0.101 \pm 0.015^{+0.022}_{-0.015}$
$2.00 \cdot 10^{-3}$	88	0.32 - 0.52	$0.130 \pm 0.053^{+0.014}_{-0.076}$
		0.52 - 0.72	$0.128 \pm 0.031^{+0.038}_{-0.049}$
		0.72 - 0.92	$0.089 \pm 0.014^{+0.021}_{-0.002}$
$3.59 \cdot 10^{-3}$	88	0.32 - 0.52	$0.126 \pm 0.037^{+0.009}_{-0.046}$
		0.52 - 0.72	$0.080 \pm 0.014^{+0.035}_{-0.004}$
		0.72 - 0.92	$0.104 \pm 0.012^{+0.015}_{-0.003}$
$7.37 \cdot 10^{-3}$	88	0.32 - 0.52	$0.091 \pm 0.031^{+0.034}_{-0.015}$
		0.52 - 0.72	$0.077 \pm 0.017^{+0.029}_{-0.006}$
		0.72 - 0.92	$0.090 \pm 0.011^{+0.026}_{-0.004}$
$1.42 \cdot 10^{-2}$	88	0.32 - 0.52	$0.075 \pm 0.024^{+0.048}_{-0.005}$
		0.52 - 0.72	$0.118 \pm 0.027^{+0.051}_{-0.010}$
		0.72 - 0.92	$0.103 \pm 0.014^{+0.034}_{-0.007}$
$3.01 \cdot 10^{-2}$	88	0.32 - 0.52	$0.151 \pm 0.075^{+0.022}_{-0.143}$
		0.52 - 0.72	$0.081 \pm 0.020^{+0.015}_{-0.012}$
		0.72 - 0.92	$0.099 \pm 0.017^{+0.033}_{-0.004}$
$4.00 \cdot 10^{-3}$	237	0.32 - 0.52	$0.053 \pm 0.036^{+0.020}_{-0.045}$
		0.52 - 0.72	$0.092 \pm 0.033^{+0.102}_{-0.006}$
		0.72 - 0.92	$0.116 \pm 0.025^{+0.022}_{-0.010}$
$7.52 \cdot 10^{-3}$	237	0.32 - 0.52	$0.116 \pm 0.052^{+0.036}_{-0.015}$
		0.52 - 0.72	$0.108 \pm 0.030^{+0.016}_{-0.057}$

Table 7 (cont.)

$\langle x \rangle$	$\langle Q^2 \rangle$ (GeV^2)	x_L range	$r^{\mathrm{LP}(3)}$
		0.72 - 0.92	$0.098 \pm 0.017^{+0.007}_{-0.024}$
$1.47 \cdot 10^{-2}$	237	0.32 - 0.52	$0.072 \pm 0.036^{+0.053}_{-0.007}$
		0.52 - 0.72	$0.098 \pm 0.025^{+0.062}_{-0.022}$
		0.72 - 0.92	$0.128 \pm 0.020^{+0.012}_{-0.025}$
$3.25 \cdot 10^{-2}$	237	0.32 - 0.52	$0.033 \pm 0.020^{+0.073}_{-0.002}$
		0.52 - 0.72	$0.071 \pm 0.019^{+0.058}_{-0.013}$
		0.72 - 0.92	$0.102 \pm 0.017^{+0.014}_{-0.019}$

$\langle x \rangle$	$\langle Q^2 \rangle$ (GeV^2)	x_L range	$r^{\mathrm{LP}(3)}$
$9.6 \cdot 10^{-5}$	4.2	0.38 - 0.56	$0.146 \pm 0.027^{+0.022}_{-0.039}$
		0.56 - 0.74	$0.125 \pm 0.012^{+0.015}_{-0.013}$
		0.74 - 0.92	$0.177 \pm 0.013^{+0.017}_{-0.058}$
$1.7 \cdot 10^{-4}$	4.2	0.38 - 0.56	$0.133 \pm 0.017^{+0.025}_{-0.026}$
		0.56 - 0.74	$0.145 \pm 0.010^{+0.006}_{-0.026}$
		0.74 - 0.92	$0.137 \pm 0.006^{+0.009}_{-0.005}$
$3.5 \cdot 10^{-4}$	4.2	0.38 - 0.56	$0.123 \pm 0.018^{+0.020}_{-0.011}$
		0.56 - 0.74	$0.140 \pm 0.009^{+0.009}_{-0.013}$
		0.74 - 0.92	$0.141 \pm 0.007^{+0.008}_{-0.012}$
$6.9 \cdot 10^{-4}$	4.2	0.38 - 0.56	$0.128 \pm 0.019^{+0.018}_{-0.028}$
		0.56 - 0.74	$0.128 \pm 0.010^{+0.008}_{-0.018}$
		0.74 - 0.92	$0.151 \pm 0.008^{+0.006}_{-0.020}$
$1.46 \cdot 10^{-3}$	4.2	0.38 - 0.56	$0.160 \pm 0.033^{+0.035}_{-0.016}$
		0.56 - 0.74	$0.156 \pm 0.018^{+0.015}_{-0.019}$
		0.74 - 0.92	$0.136 \pm 0.010^{+0.017}_{-0.020}$
$1.9 \cdot 10^{-4}$	7.3	0.38 - 0.56	$0.126 \pm 0.023^{+0.048}_{-0.006}$
		0.56 - 0.74	$0.123 \pm 0.012^{+0.009}_{-0.016}$
		0.74 - 0.92	$0.149 \pm 0.011^{+0.004}_{-0.020}$
$3.4 \cdot 10^{-4}$	7.3	0.38 - 0.56	$0.140 \pm 0.022^{+0.018}_{-0.028}$
		0.56 - 0.74	$0.144 \pm 0.012^{+0.006}_{-0.026}$
		0.74 - 0.92	$0.136 \pm 0.008^{+0.008}_{-0.008}$
$6.9 \cdot 10^{-4}$	7.3	0.38 - 0.56	$0.123 \pm 0.021^{+0.019}_{-0.022}$
		0.56 - 0.74	$0.122 \pm 0.011^{+0.012}_{-0.004}$
		0.74 - 0.92	$0.141 \pm 0.008^{+0.009}_{-0.014}$
$1.36 \cdot 10^{-3}$	7.3	0.38 - 0.56	$0.158 \pm 0.027^{+0.052}_{-0.024}$
		0.56 - 0.74	$0.140 \pm 0.013^{+0.016}_{-0.009}$
		0.74 - 0.92	$0.149 \pm 0.010^{+0.013}_{-0.006}$
$2.67 \cdot 10^{-3}$	7.3	0.38 - 0.56	$0.175 \pm 0.070^{+0.023}_{-0.153}$
		0.56 - 0.74	$0.193 \pm 0.038^{+0.077}_{-0.054}$
		0.74 - 0.92	$0.161 \pm 0.021^{+0.032}_{-0.024}$

Table 8: *The leading-proton production rate $r^{\mathrm{LP}(3)}$ measured as a function of x_L for protons with $0.04 < p_T^2 < 0.15$ GeV^2, in bins of x and Q^2, with averages $\langle x \rangle$ and $\langle Q^2 \rangle$. Statistical uncertainties are listed first, followed by systematic uncertainties.*

Table 8 (cont.)

$\langle x \rangle$	$\langle Q^2 \rangle$ (GeV^2)	x_L range	$r^{\mathrm{LP}(3)}$
$2.6 \cdot 10^{-4}$	11	0.38 - 0.56	$0.084 \pm 0.021^{+0.033}_{-0.008}$
		0.56 - 0.74	$0.151 \pm 0.019^{+0.010}_{-0.030}$
		0.74 - 0.92	$0.140 \pm 0.012^{+0.013}_{-0.006}$
$4.6 \cdot 10^{-4}$	11	0.38 - 0.56	$0.134 \pm 0.020^{+0.056}_{-0.009}$
		0.56 - 0.74	$0.132 \pm 0.011^{+0.009}_{-0.016}$
		0.74 - 0.92	$0.133 \pm 0.007^{+0.032}_{-0.003}$
$9.2 \cdot 10^{-4}$	11	0.38 - 0.56	$0.129 \pm 0.021^{+0.008}_{-0.015}$
		0.56 - 0.74	$0.140 \pm 0.011^{+0.032}_{-0.006}$
		0.74 - 0.92	$0.150 \pm 0.008^{+0.003}_{-0.022}$
$1.83 \cdot 10^{-3}$	11	0.38 - 0.56	$0.115 \pm 0.018^{+0.026}_{-0.007}$
		0.56 - 0.74	$0.165 \pm 0.013^{+0.007}_{-0.036}$
		0.74 - 0.92	$0.127 \pm 0.007^{+0.022}_{-0.003}$
$3.98 \cdot 10^{-3}$	11	0.38 - 0.56	$0.110 \pm 0.031^{+0.099}_{-0.013}$
		0.56 - 0.74	$0.129 \pm 0.018^{+0.007}_{-0.032}$
		0.74 - 0.92	$0.157 \pm 0.013^{+0.018}_{-0.024}$
$5.1 \cdot 10^{-4}$	22	0.38 - 0.56	$0.112 \pm 0.029^{+0.079}_{-0.009}$
		0.56 - 0.74	$0.133 \pm 0.017^{+0.009}_{-0.019}$
		0.74 - 0.92	$0.148 \pm 0.013^{+0.037}_{-0.003}$
$9.2 \cdot 10^{-4}$	22	0.38 - 0.56	$0.146 \pm 0.028^{+0.039}_{-0.025}$
		0.56 - 0.74	$0.153 \pm 0.015^{+0.007}_{-0.025}$
		0.74 - 0.92	$0.157 \pm 0.010^{+0.004}_{-0.016}$
$1.84 \cdot 10^{-3}$	22	0.38 - 0.56	$0.101 \pm 0.019^{+0.050}_{-0.006}$
		0.56 - 0.74	$0.141 \pm 0.013^{+0.009}_{-0.012}$
		0.74 - 0.92	$0.144 \pm 0.009^{+0.019}_{-0.006}$
$3.66 \cdot 10^{-3}$	22	0.38 - 0.56	$0.177 \pm 0.036^{+0.042}_{-0.018}$
		0.56 - 0.74	$0.165 \pm 0.018^{+0.014}_{-0.020}$
		0.74 - 0.92	$0.156 \pm 0.011^{+0.005}_{-0.020}$
$7.83 \cdot 10^{-3}$	22	0.38 - 0.56	$0.166 \pm 0.046^{+0.063}_{-0.014}$
		0.56 - 0.74	$0.185 \pm 0.031^{+0.011}_{-0.065}$
		0.74 - 0.92	$0.147 \pm 0.015^{+0.007}_{-0.023}$
$1.03 \cdot 10^{-3}$	44	0.38 - 0.56	$0.128 \pm 0.042^{+0.155}_{-0.008}$
		0.56 - 0.74	$0.090 \pm 0.016^{+0.052}_{-0.006}$

Table 8 (cont.)

$\langle x \rangle$	$\langle Q^2 \rangle$ (GeV^2)	x_L range	$r^{\mathrm{LP}(3)}$
		0.74 - 0.92	$0.152 \pm 0.018^{+0.005}_{-0.042}$
$1.86 \cdot 10^{-3}$	44	0.38 - 0.56	$0.190 \pm 0.048^{+0.059}_{-0.015}$
		0.56 - 0.74	$0.136 \pm 0.019^{+0.006}_{-0.029}$
		0.74 - 0.92	$0.115 \pm 0.010^{+0.049}_{-0.003}$
$3.68 \cdot 10^{-3}$	44	0.38 - 0.56	$0.082 \pm 0.023^{+0.176}_{-0.010}$
		0.56 - 0.74	$0.156 \pm 0.023^{+0.017}_{-0.031}$
		0.74 - 0.92	$0.158 \pm 0.015^{+0.021}_{-0.004}$
$7.33 \cdot 10^{-3}$	44	0.38 - 0.56	$0.138 \pm 0.045^{+0.070}_{-0.011}$
		0.56 - 0.74	$0.169 \pm 0.028^{+0.027}_{-0.022}$
		0.74 - 0.92	$0.188 \pm 0.020^{+0.010}_{-0.056}$
$1.54 \cdot 10^{-2}$	44	0.38 - 0.56	$0.130 \pm 0.055^{+0.056}_{-0.036}$
		0.56 - 0.74	$0.195 \pm 0.043^{+0.042}_{-0.078}$
		0.74 - 0.92	$0.118 \pm 0.016^{+0.052}_{-0.004}$
$2.00 \cdot 10^{-3}$	88	0.38 - 0.65	$0.092 \pm 0.030^{+0.025}_{-0.018}$
		0.65 - 0.92	$0.109 \pm 0.018^{+0.020}_{-0.009}$
$3.59 \cdot 10^{-3}$	88	0.38 - 0.65	$0.236 \pm 0.053^{+0.030}_{-0.098}$
		0.65 - 0.92	$0.153 \pm 0.018^{+0.018}_{-0.006}$
$7.37 \cdot 10^{-3}$	88	0.38 - 0.65	$0.190 \pm 0.047^{+0.078}_{-0.030}$
		0.65 - 0.92	$0.191 \pm 0.024^{+0.022}_{-0.047}$
$1.42 \cdot 10^{-2}$	88	0.38 - 0.65	$0.153 \pm 0.040^{+0.072}_{-0.018}$
		0.65 - 0.92	$0.179 \pm 0.026^{+0.004}_{-0.063}$
$3.01 \cdot 10^{-2}$	88	0.38 - 0.65	$0.137 \pm 0.053^{+0.095}_{-0.010}$
		0.65 - 0.92	$0.158 \pm 0.032^{+0.030}_{-0.026}$
$4.00 \cdot 10^{-3}$	237	0.38 - 0.65	$0.051 \pm 0.048^{+0.119}_{-0.003}$
		0.65 - 0.92	$0.067 \pm 0.027^{+0.069}_{-0.012}$
$7.52 \cdot 10^{-3}$	237	0.38 - 0.65	$0.162 \pm 0.053^{+0.023}_{-0.048}$
		0.65 - 0.92	$0.164 \pm 0.027^{+0.094}_{-0.036}$
$1.47 \cdot 10^{-2}$	237	0.38 - 0.65	$0.161 \pm 0.052^{+0.049}_{-0.048}$
		0.65 - 0.92	$0.095 \pm 0.015^{+0.056}_{-0.005}$
$3.25 \cdot 10^{-2}$	237	0.38 - 0.65	$0.179 \pm 0.054^{+0.026}_{-0.056}$
		0.65 - 0.92	$0.123 \pm 0.019^{+0.017}_{-0.008}$

$\langle x \rangle$	$\langle Q^2 \rangle$ (GeV^2)	x_L range	$r^{\mathrm{LP}(3)}$
$9.6 \cdot 10^{-5}$	4.2	0.62 - 0.72	$0.114 \pm 0.027^{+0.072}_{-0.014}$
		0.72 - 0.82	$0.116 \pm 0.033^{+0.066}_{-0.026}$
		0.82 - 0.92	$0.121 \pm 0.016^{+0.054}_{-0.015}$
$1.7 \cdot 10^{-4}$	4.2	0.62 - 0.72	$0.102 \pm 0.014^{+0.018}_{-0.026}$
		0.72 - 0.82	$0.105 \pm 0.018^{+0.053}_{-0.034}$
		0.82 - 0.92	$0.133 \pm 0.012^{+0.036}_{-0.011}$
$3.5 \cdot 10^{-4}$	4.2	0.62 - 0.72	$0.114 \pm 0.018^{+0.010}_{-0.021}$
		0.72 - 0.82	$0.212 \pm 0.043^{+0.023}_{-0.172}$
		0.82 - 0.92	$0.099 \pm 0.010^{+0.010}_{-0.011}$
$6.9 \cdot 10^{-4}$	4.2	0.62 - 0.72	$0.097 \pm 0.015^{+0.040}_{-0.007}$
		0.72 - 0.82	$0.166 \pm 0.034^{+0.036}_{-0.048}$
		0.82 - 0.92	$0.151 \pm 0.016^{+0.011}_{-0.020}$
$1.46 \cdot 10^{-3}$	4.2	0.62 - 0.72	$0.106 \pm 0.024^{+0.015}_{-0.022}$
		0.72 - 0.82	$0.090 \pm 0.027^{+0.021}_{-0.039}$
		0.82 - 0.92	$0.154 \pm 0.022^{+0.043}_{-0.033}$
$1.9 \cdot 10^{-4}$	7.3	0.62 - 0.72	$0.158 \pm 0.034^{+0.012}_{-0.069}$
		0.72 - 0.82	$0.068 \pm 0.026^{+0.030}_{-0.040}$
		0.82 - 0.92	$0.100 \pm 0.017^{+0.019}_{-0.035}$
$3.4 \cdot 10^{-4}$	7.3	0.62 - 0.72	$0.138 \pm 0.025^{+0.013}_{-0.025}$
		0.72 - 0.82	$0.149 \pm 0.034^{+0.020}_{-0.077}$
		0.82 - 0.92	$0.110 \pm 0.013^{+0.012}_{-0.017}$
$6.9 \cdot 10^{-4}$	7.3	0.62 - 0.72	$0.137 \pm 0.025^{+0.010}_{-0.042}$
		0.72 - 0.82	$0.098 \pm 0.024^{+0.009}_{-0.035}$
		0.82 - 0.92	$0.160 \pm 0.018^{+0.012}_{-0.032}$
$1.36 \cdot 10^{-3}$	7.3	0.62 - 0.72	$0.127 \pm 0.024^{+0.038}_{-0.008}$
		0.72 - 0.82	$0.170 \pm 0.040^{+0.068}_{-0.066}$
		0.82 - 0.92	$0.127 \pm 0.016^{+0.009}_{-0.023}$
$2.67 \cdot 10^{-3}$	7.3	0.62 - 0.77	$0.245 \pm 0.103^{+0.119}_{-0.120}$
		0.77 - 0.92	$0.113 \pm 0.027^{+0.060}_{-0.018}$

Table 9: *The leading-proton production rate $r^{\mathrm{LP}(3)}$ measured as a function of x_L for protons with $0.15 < p_T^2 < 0.5$ GeV^2, in bins of x and Q^2, with averages $\langle x \rangle$ and $\langle Q^2 \rangle$. Statistical uncertainties are listed first, followed by systematic uncertainties.*

Table 9 (cont.)

$\langle x \rangle$	$\langle Q^2 \rangle$ (GeV^2)	x_L range	$r^{\mathrm{LP}(3)}$
$2.6 \cdot 10^{-4}$	11	0.62 - 0.72	$0.170 \pm 0.047^{+0.063}_{-0.036}$
		0.72 - 0.82	$0.088 \pm 0.048^{+0.225}_{-0.012}$
		0.82 - 0.92	$0.169 \pm 0.027^{+0.023}_{-0.059}$
$4.6 \cdot 10^{-4}$	11	0.62 - 0.72	$0.176 \pm 0.030^{+0.015}_{-0.040}$
		0.72 - 0.82	$0.126 \pm 0.030^{+0.076}_{-0.074}$
		0.82 - 0.92	$0.134 \pm 0.015^{+0.020}_{-0.027}$
$9.2 \cdot 10^{-4}$	11	0.62 - 0.72	$0.142 \pm 0.023^{+0.015}_{-0.039}$
		0.72 - 0.82	$0.158 \pm 0.040^{+0.026}_{-0.117}$
		0.82 - 0.92	$0.148 \pm 0.016^{+0.017}_{-0.019}$
$1.83 \cdot 10^{-3}$	11	0.62 - 0.72	$0.107 \pm 0.018^{+0.018}_{-0.012}$
		0.72 - 0.82	$0.071 \pm 0.019^{+0.089}_{-0.008}$
		0.82 - 0.92	$0.145 \pm 0.015^{+0.020}_{-0.017}$
$3.98 \cdot 10^{-3}$	11	0.62 - 0.77	$0.135 \pm 0.034^{+0.058}_{-0.014}$
		0.77 - 0.92	$0.199 \pm 0.033^{+0.018}_{-0.050}$
$5.1 \cdot 10^{-4}$	22	0.62 - 0.72	$0.125 \pm 0.033^{+0.019}_{-0.052}$
		0.72 - 0.82	$0.179 \pm 0.069^{+0.038}_{-0.121}$
		0.82 - 0.92	$0.127 \pm 0.020^{+0.053}_{-0.012}$
$9.2 \cdot 10^{-4}$	22	0.62 - 0.72	$0.127 \pm 0.024^{+0.057}_{-0.016}$
		0.72 - 0.82	$0.106 \pm 0.027^{+0.014}_{-0.019}$
		0.82 - 0.92	$0.147 \pm 0.018^{+0.010}_{-0.021}$
$1.84 \cdot 10^{-3}$	22	0.62 - 0.72	$0.084 \pm 0.017^{+0.028}_{-0.008}$
		0.72 - 0.82	$0.158 \pm 0.039^{+0.017}_{-0.063}$
		0.82 - 0.92	$0.157 \pm 0.021^{+0.016}_{-0.036}$
$3.66 \cdot 10^{-3}$	22	0.62 - 0.72	$0.115 \pm 0.029^{+0.019}_{-0.052}$
		0.72 - 0.82	$0.112 \pm 0.030^{+0.097}_{-0.011}$
		0.82 - 0.92	$0.124 \pm 0.020^{+0.018}_{-0.068}$
$7.83 \cdot 10^{-3}$	22	0.62 - 0.77	$0.110 \pm 0.037^{+0.064}_{-0.024}$
		0.77 - 0.92	$0.223 \pm 0.044^{+0.015}_{-0.127}$
$1.03 \cdot 10^{-3}$	44	0.62 - 0.77	$0.171 \pm 0.054^{+0.048}_{-0.039}$
		0.77 - 0.92	$0.100 \pm 0.023^{+0.014}_{-0.024}$
$1.86 \cdot 10^{-3}$	44	0.62 - 0.77	$0.124 \pm 0.030^{+0.013}_{-0.024}$
		0.77 - 0.92	$0.141 \pm 0.022^{+0.068}_{-0.015}$

Table 9 (cont.)

$\langle x \rangle$	$\langle Q^2 \rangle$ (GeV^2)	x_L range	$r^{\mathrm{LP}(3)}$
$3.68 \cdot 10^{-3}$	44	0.62 - 0.77	$0.170 \pm 0.049^{+0.060}_{-0.058}$
		0.77 - 0.92	$0.117 \pm 0.022^{+0.026}_{-0.016}$
$7.33 \cdot 10^{-3}$	44	0.62 - 0.77	$0.185 \pm 0.078^{+0.044}_{-0.103}$
		0.77 - 0.92	$0.120 \pm 0.024^{+0.037}_{-0.074}$
$1.54 \cdot 10^{-2}$	44	0.62 - 0.77	$0.196 \pm 0.078^{+0.228}_{-0.020}$
		0.77 - 0.92	$0.182 \pm 0.050^{+0.041}_{-0.079}$
$2.00 \cdot 10^{-3}$	88	0.62 - 0.77	$0.156 \pm 0.077^{+0.040}_{-0.081}$
		0.77 - 0.92	$0.125 \pm 0.034^{+0.011}_{-0.047}$
$3.59 \cdot 10^{-3}$	88	0.62 - 0.77	$0.208 \pm 0.087^{+0.115}_{-0.044}$
		0.77 - 0.92	$0.129 \pm 0.027^{+0.067}_{-0.019}$
$7.37 \cdot 10^{-3}$	88	0.62 - 0.77	$0.061 \pm 0.031^{+0.003}_{-0.022}$
		0.77 - 0.92	$0.127 \pm 0.035^{+0.050}_{-0.040}$
$1.42 \cdot 10^{-2}$	88	0.62 - 0.77	$0.145 \pm 0.056^{+0.338}_{-0.013}$
		0.77 - 0.92	$0.268 \pm 0.079^{+0.030}_{-0.264}$
$3.01 \cdot 10^{-2}$	88	0.62 - 0.77	$0.106 \pm 0.063^{+0.200}_{-0.040}$
		0.77 - 0.92	$0.215 \pm 0.107^{+0.031}_{-0.146}$
$4.00 \cdot 10^{-3}$	237	0.62 - 0.92	$0.248 \pm 0.107^{+0.024}_{-0.132}$
$7.52 \cdot 10^{-3}$	237	0.62 - 0.92	$0.183 \pm 0.049^{+0.068}_{-0.027}$
$1.47 \cdot 10^{-2}$	237	0.62 - 0.92	$0.203 \pm 0.057^{+0.016}_{-0.059}$
$3.25 \cdot 10^{-2}$	237	0.62 - 0.92	$0.164 \pm 0.045^{+0.061}_{-0.055}$

$\langle Q^2 \rangle$ (GeV^2)	x	$r^{\mathrm{LP}(2)}$
4.2	$9.6 \cdot 10^{-5}$	$0.256 \pm 0.006^{+0.023}_{-0.022}$
	$1.7 \cdot 10^{-4}$	$0.245 \pm 0.004^{+0.018}_{-0.021}$
	$3.5 \cdot 10^{-4}$	$0.237 \pm 0.004^{+0.018}_{-0.017}$
	$6.9 \cdot 10^{-4}$	$0.234 \pm 0.004^{+0.018}_{-0.016}$
	$1.46 \cdot 10^{-3}$	$0.214 \pm 0.006^{+0.020}_{-0.016}$
7.3	$1.9 \cdot 10^{-4}$	$0.246 \pm 0.006^{+0.020}_{-0.024}$
	$3.4 \cdot 10^{-4}$	$0.231 \pm 0.005^{+0.019}_{-0.016}$
	$6.9 \cdot 10^{-4}$	$0.236 \pm 0.005^{+0.018}_{-0.021}$
	$1.36 \cdot 10^{-3}$	$0.243 \pm 0.006^{+0.019}_{-0.018}$
	$2.67 \cdot 10^{-3}$	$0.252 \pm 0.012^{+0.025}_{-0.030}$
11	$2.6 \cdot 10^{-4}$	$0.253 \pm 0.007^{+0.020}_{-0.016}$
	$4.6 \cdot 10^{-4}$	$0.241 \pm 0.005^{+0.020}_{-0.015}$
	$9.2 \cdot 10^{-4}$	$0.242 \pm 0.005^{+0.018}_{-0.019}$
	$1.83 \cdot 10^{-3}$	$0.230 \pm 0.005^{+0.019}_{-0.014}$
	$3.98 \cdot 10^{-3}$	$0.258 \pm 0.008^{+0.019}_{-0.030}$
22	$5.1 \cdot 10^{-4}$	$0.242 \pm 0.007^{+0.020}_{-0.023}$
	$9.2 \cdot 10^{-4}$	$0.244 \pm 0.006^{+0.018}_{-0.018}$
	$1.84 \cdot 10^{-4}$	$0.227 \pm 0.005^{+0.022}_{-0.016}$
	$3.66 \cdot 10^{-3}$	$0.253 \pm 0.007^{+0.020}_{-0.018}$
	$7.83 \cdot 10^{-3}$	$0.254 \pm 0.010^{+0.025}_{-0.020}$
44	$1.03 \cdot 10^{-3}$	$0.228 \pm 0.009^{+0.017}_{-0.015}$
	$1.86 \cdot 10^{-3}$	$0.238 \pm 0.008^{+0.019}_{-0.016}$
	$3.68 \cdot 10^{-3}$	$0.270 \pm 0.009^{+0.020}_{-0.021}$
	$7.33 \cdot 10^{-3}$	$0.271 \pm 0.011^{+0.023}_{-0.017}$
	$1.54 \cdot 10^{-3}$	$0.253 \pm 0.014^{+0.031}_{-0.016}$
88	$2.00 \cdot 10^{-3}$	$0.215 \pm 0.013^{+0.015}_{-0.019}$
	$3.59 \cdot 10^{-3}$	$0.245 \pm 0.011^{+0.043}_{-0.017}$
	$7.37 \cdot 10^{-3}$	$0.243 \pm 0.013^{+0.026}_{-0.017}$
	$1.42 \cdot 10^{-2}$	$0.265 \pm 0.015^{+0.032}_{-0.023}$
	$3.01 \cdot 10^{-2}$	$0.241 \pm 0.019^{+0.034}_{-0.024}$
237	$4.00 \cdot 10^{-2}$	$0.242 \pm 0.024^{+0.069}_{-0.021}$
	$7.52 \cdot 10^{-2}$	$0.264 \pm 0.018^{+0.029}_{-0.038}$
	$1.47 \cdot 10^{-2}$	$0.227 \pm 0.015^{+0.029}_{-0.017}$
	$3.25 \cdot 10^{-2}$	$0.232 \pm 0.015^{+0.021}_{-0.019}$

Table 10: *The leading-proton production rate $r^{\mathrm{LP}(2)}$ measured as a function of x in bins of Q^2, with average $\langle Q^2 \rangle$, for protons with $0.32 < x_L < 0.92$ and $p_T^2 < 0.5$ GeV^2. Statistical uncertainties are listed first, followed by systematic uncertainties.*

Q^2 (GeV^2)	$\langle r^{\mathrm{LP(2)}} \rangle$	
	$0.6 < x_L < 0.97$	$0.32 < x_L < 0.92$
5.1	$0.145 \pm 0.001^{+0.010}_{-0.010}$	$0.238 \pm 0.002^{+0.018}_{-0.017}$
15.8	$0.149 \pm 0.001^{+0.011}_{-0.009}$	$0.241 \pm 0.002^{+0.018}_{-0.015}$
81.1	$0.151 \pm 0.002^{+0.011}_{-0.009}$	$0.245 \pm 0.003^{+0.019}_{-0.015}$

Table 11: *The leading-proton production rate $\langle r^{\mathrm{LP(2)}} \rangle$, averaged over x, as a function of Q^2, for protons with $p_T^2 < 0.5$ GeV^2 in two x_L ranges as denoted in the table. Statistical uncertainties are listed first, followed by systematic uncertainties.*

$\langle Q^2 \rangle$ (GeV^2)	x	$F_2^{\mathrm{LP}(2)}$
4.2	$9.6 \cdot 10^{-5}$	$0.262 \pm 0.006^{+0.023}_{-0.024}$
	$1.7 \cdot 10^{-4}$	$0.234 \pm 0.004^{+0.021}_{-0.018}$
	$3.5 \cdot 10^{-4}$	$0.195 \pm 0.003^{+0.015}_{-0.015}$
	$6.9 \cdot 10^{-4}$	$0.167 \pm 0.003^{+0.012}_{-0.013}$
	$1.46 \cdot 10^{-3}$	$0.133 \pm 0.004^{+0.011}_{-0.013}$
7.3	$1.9 \cdot 10^{-4}$	$0.290 \pm 0.007^{+0.030}_{-0.024}$
	$3.4 \cdot 10^{-4}$	$0.239 \pm 0.005^{+0.018}_{-0.020}$
	$6.9 \cdot 10^{-4}$	$0.209 \pm 0.004^{+0.019}_{-0.016}$
	$1.36 \cdot 10^{-3}$	$0.183 \pm 0.004^{+0.014}_{-0.015}$
	$2.67 \cdot 10^{-3}$	$0.165 \pm 0.008^{+0.021}_{-0.018}$
11	$2.6 \cdot 10^{-4}$	$0.327 \pm 0.010^{+0.023}_{-0.027}$
	$4.6 \cdot 10^{-4}$	$0.281 \pm 0.005^{+0.018}_{-0.024}$
	$9.2 \cdot 10^{-4}$	$0.239 \pm 0.005^{+0.020}_{-0.019}$
	$1.83 \cdot 10^{-3}$	$0.191 \pm 0.004^{+0.012}_{-0.017}$
	$3.98 \cdot 10^{-3}$	$0.181 \pm 0.006^{+0.022}_{-0.015}$
22	$5.1 \cdot 10^{-4}$	$0.336 \pm 0.010^{+0.033}_{-0.030}$
	$9.2 \cdot 10^{-4}$	$0.299 \pm 0.007^{+0.023}_{-0.023}$
	$1.84 \cdot 10^{-3}$	$0.230 \pm 0.005^{+0.017}_{-0.023}$
	$3.66 \cdot 10^{-3}$	$0.210 \pm 0.006^{+0.016}_{-0.018}$
	$7.83 \cdot 10^{-3}$	$0.176 \pm 0.007^{+0.015}_{-0.018}$
44	$1.03 \cdot 10^{-4}$	$0.322 \pm 0.013^{+0.025}_{-0.027}$
	$1.86 \cdot 10^{-3}$	$0.286 \pm 0.009^{+0.022}_{-0.025}$
	$3.68 \cdot 10^{-3}$	$0.265 \pm 0.009^{+0.023}_{-0.022}$
	$7.33 \cdot 10^{-3}$	$0.215 \pm 0.008^{+0.016}_{-0.020}$
	$1.54 \cdot 10^{-2}$	$0.164 \pm 0.009^{+0.014}_{-0.022}$
88	$2.00 \cdot 10^{-3}$	$0.286 \pm 0.017^{+0.030}_{-0.027}$
	$3.59 \cdot 10^{-3}$	$0.275 \pm 0.013^{+0.023}_{-0.050}$
	$7.37 \cdot 10^{-3}$	$0.214 \pm 0.011^{+0.018}_{-0.026}$
	$1.42 \cdot 10^{-2}$	$0.190 \pm 0.010^{+0.020}_{-0.025}$
	$3.01 \cdot 10^{-2}$	$0.138 \pm 0.011^{+0.017}_{-0.022}$
273	$4.00 \cdot 10^{-3}$	$0.287 \pm 0.028^{+0.038}_{-0.087}$
	$7.52 \cdot 10^{-3}$	$0.260 \pm 0.017^{+0.041}_{-0.034}$
	$1.47 \cdot 10^{-2}$	$0.173 \pm 0.012^{+0.017}_{-0.025}$
	$3.25 \cdot 10^{-2}$	$0.139 \pm 0.009^{+0.015}_{-0.016}$

Table 12: *The leading-proton structure function $F_2^{\mathrm{LP}(2)}$ measured as a function of x in bins of Q^2, with average $\langle Q^2 \rangle$, for protons with $0.32 < x_L < 0.92$ and $p_T^2 < 0.5$ GeV^2. Statistical uncertainties are listed first, followed by systematic uncertainties.*

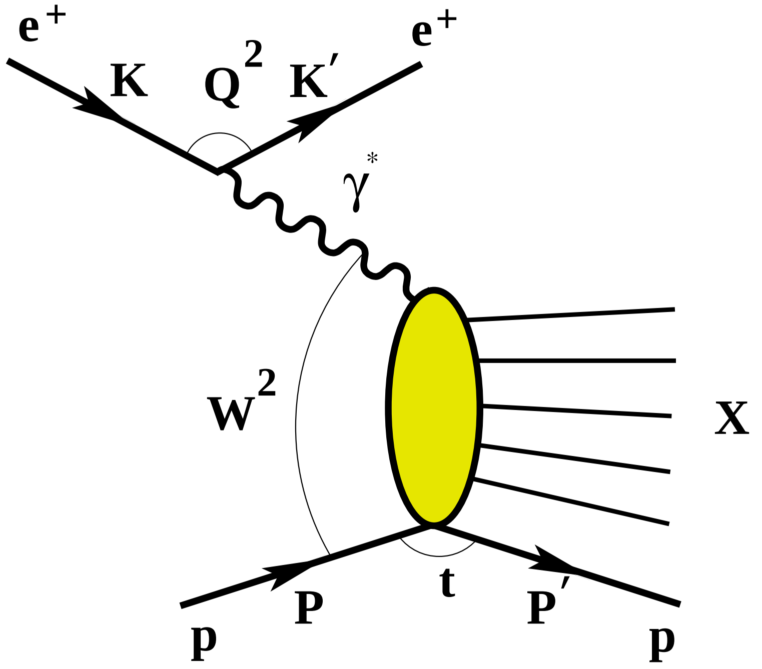

Figure 1: *Schematic diagram of the reaction $e^+p \to e^+Xp$.*

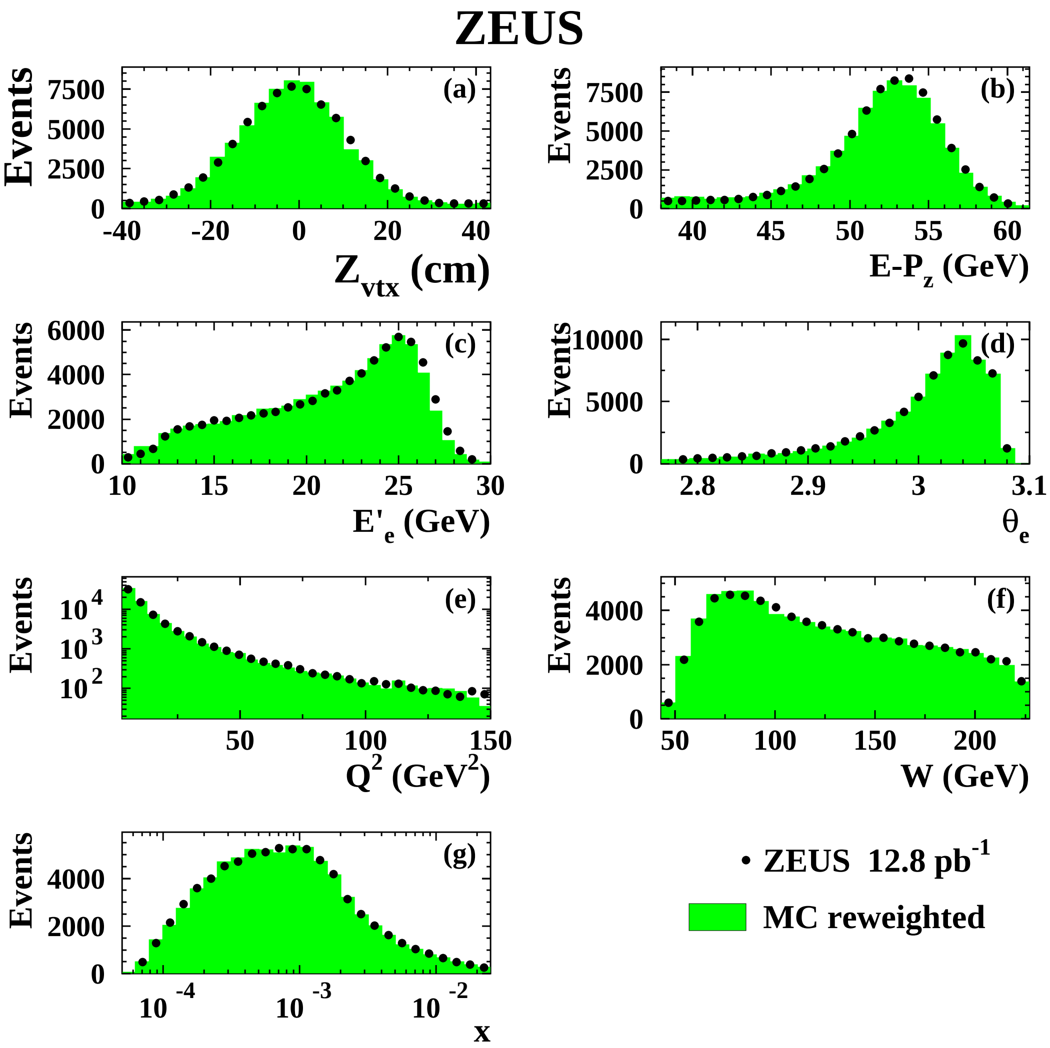

Figure 2: *Comparison between data (dots) and reweighted MC (shaded histograms) for DIS quantities for the LPS sample: (a) Z coordinate of the vertex, (b) $E - P_Z$ distribution, (c) energy of the scattered positron, E'_e, (d) polar angle of the scattered positron, θ_e, (e) virtuality of the exchanged photon, Q^2, (f) invariant mass of the hadronic system, W, (g) Bjorken scaling variable, x.*

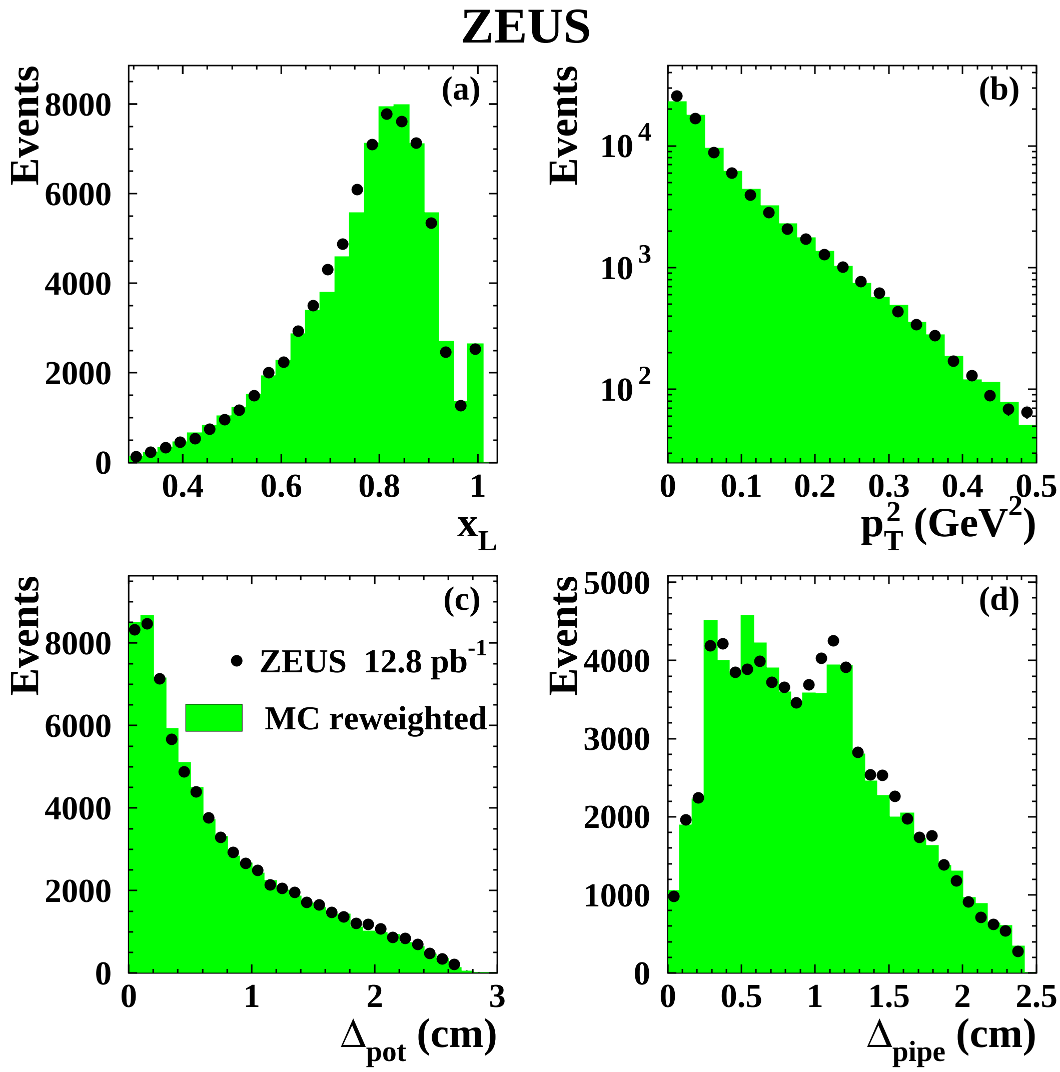

Figure 3: *Comparison between data (dots) and reweighted MC (shaded histograms) for LPS specific quantities: (a) fractional longitudinal momentum, x_L, (b) squared transverse momentum, p_T^2, (c) minimum track distance from the edge of the pot, $\Delta_{\rm pot}$, (d) minimum track distance from the beampipe, $\Delta_{\rm pipe}$.*

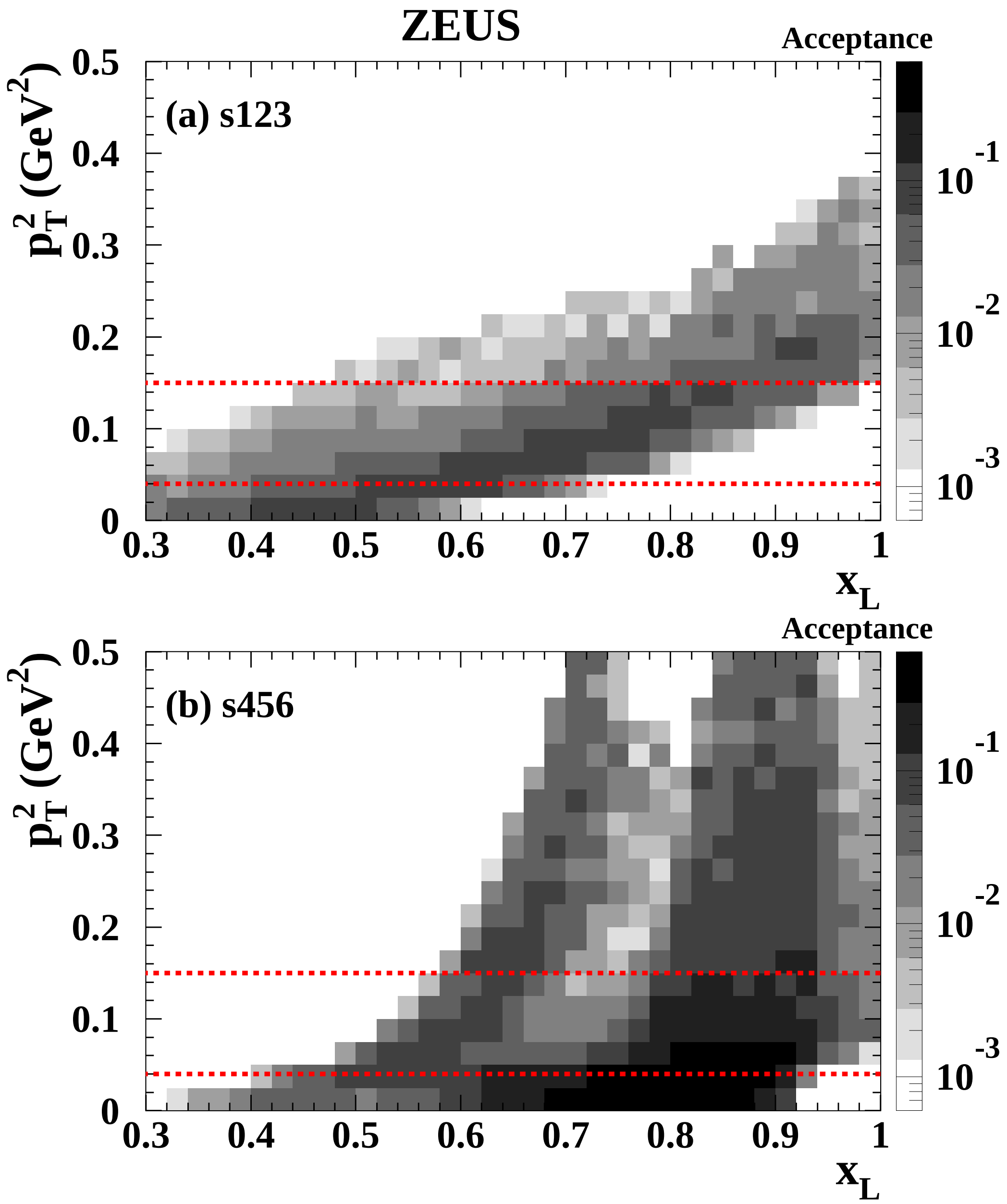

Figure 4: *Acceptance of the LPS spectrometers (a) s123 and (b) s456 in the x_L, p_T^2 plane. The dashed lines delimit the three p_T^2 integration ranges.*

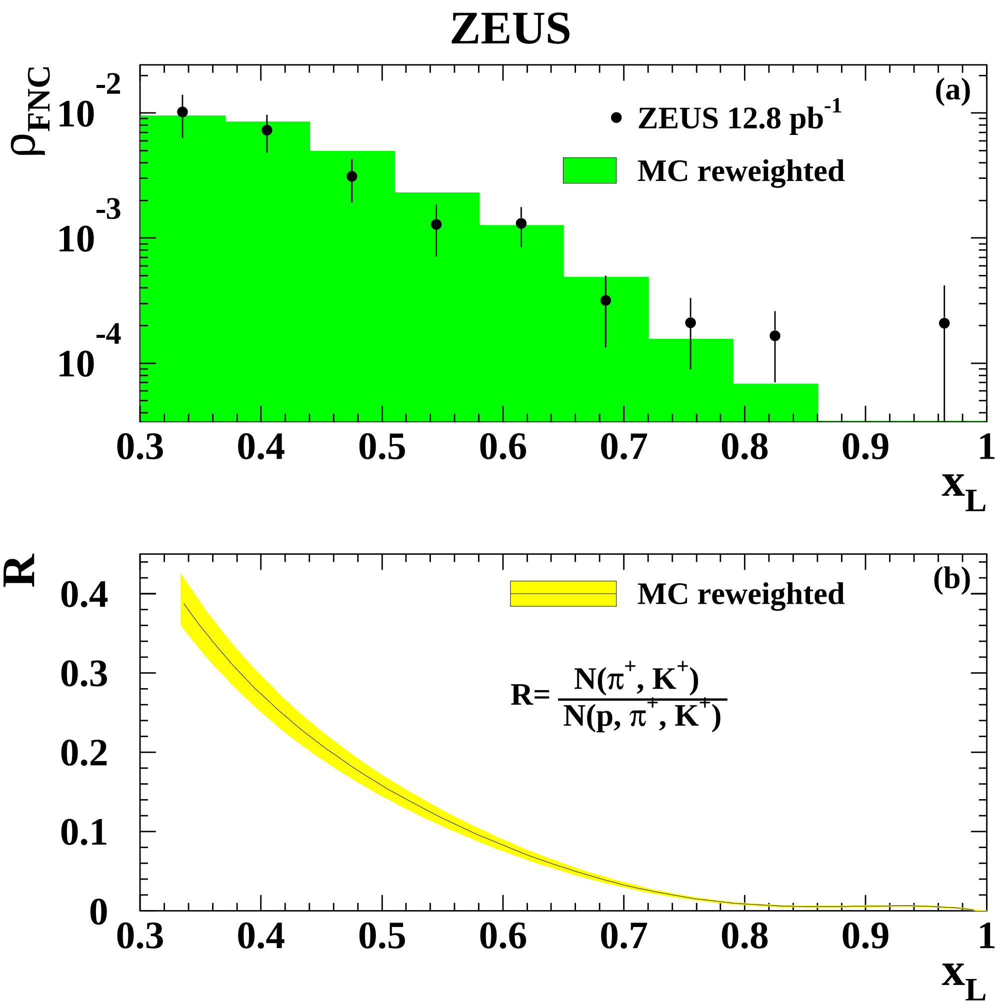

Figure 5: *(a) Ratio ρ_{FNC} of the number of events with a track in the LPS and a neutron candidate in the FNC to the number of events with a track in the LPS. The dots represent the data and the shaded histogram the reweighted MC; (b) expected fraction R of positive pions and kaons reconstructed in the LPS as a function of x_L. The error band reflects the statistical uncertainty derived from the LPS-FNC data sample.*

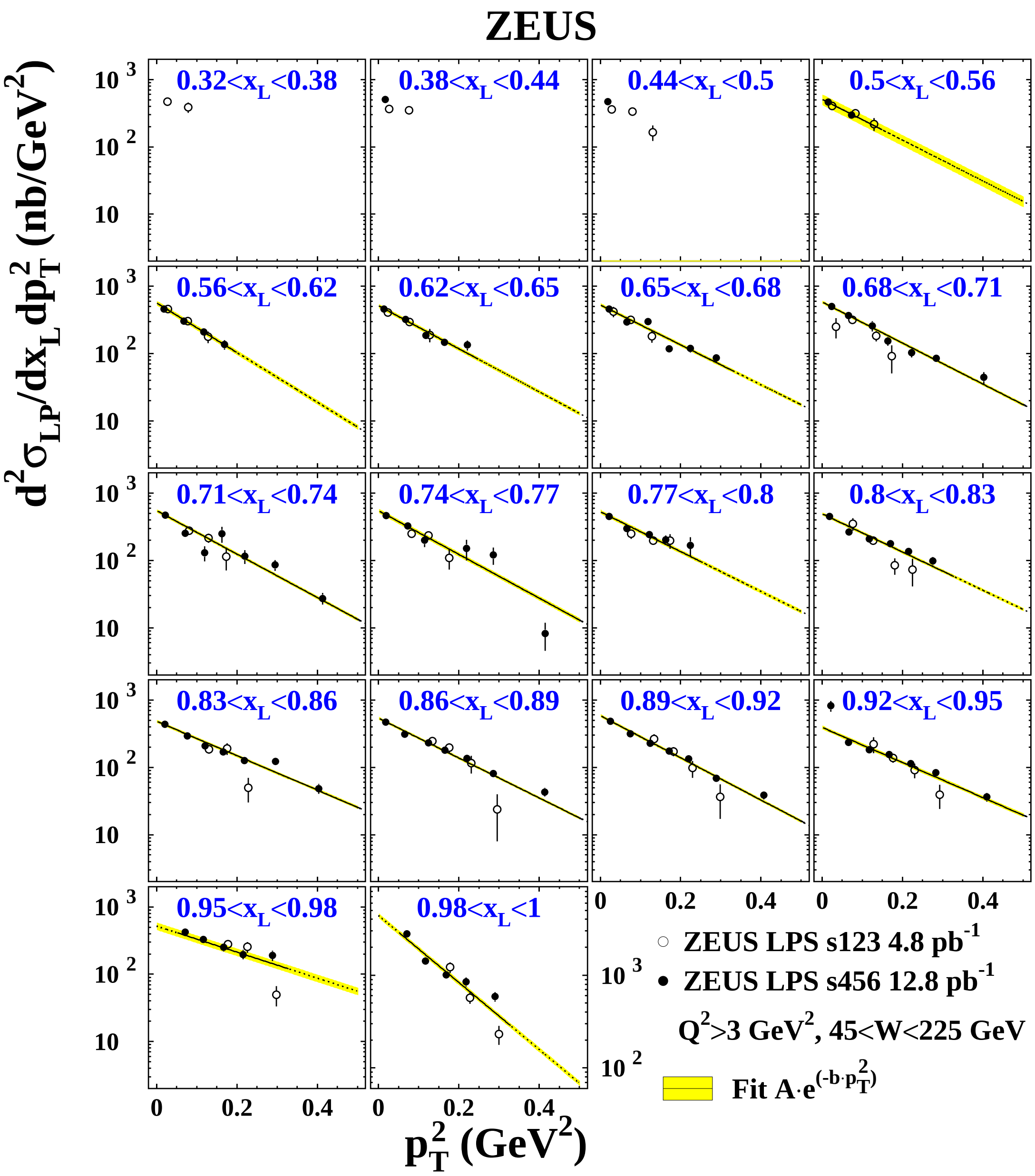

Figure 6: *The double-differential cross section $d^2\sigma_{\rm LP}/dx_L dp_T^2$ for $Q^2 > 3$ GeV^2 and $45 < W < 225$ GeV as a function of p_T^2 in bins of x_L. The circles and the dots are the ZEUS data measured with the spectrometers s123 and s456, respectively. For the sake of clarity, only the statistical uncertainties are shown. The systematic uncertainties are listed in Table 1. The lines are the result of a fit to the data of a function $A \cdot e^{-b \cdot p_T^2}$, as described in the text. The solid lines indicate the range in which the fit was performed. The bands show the statistical uncertainty of the fit.*

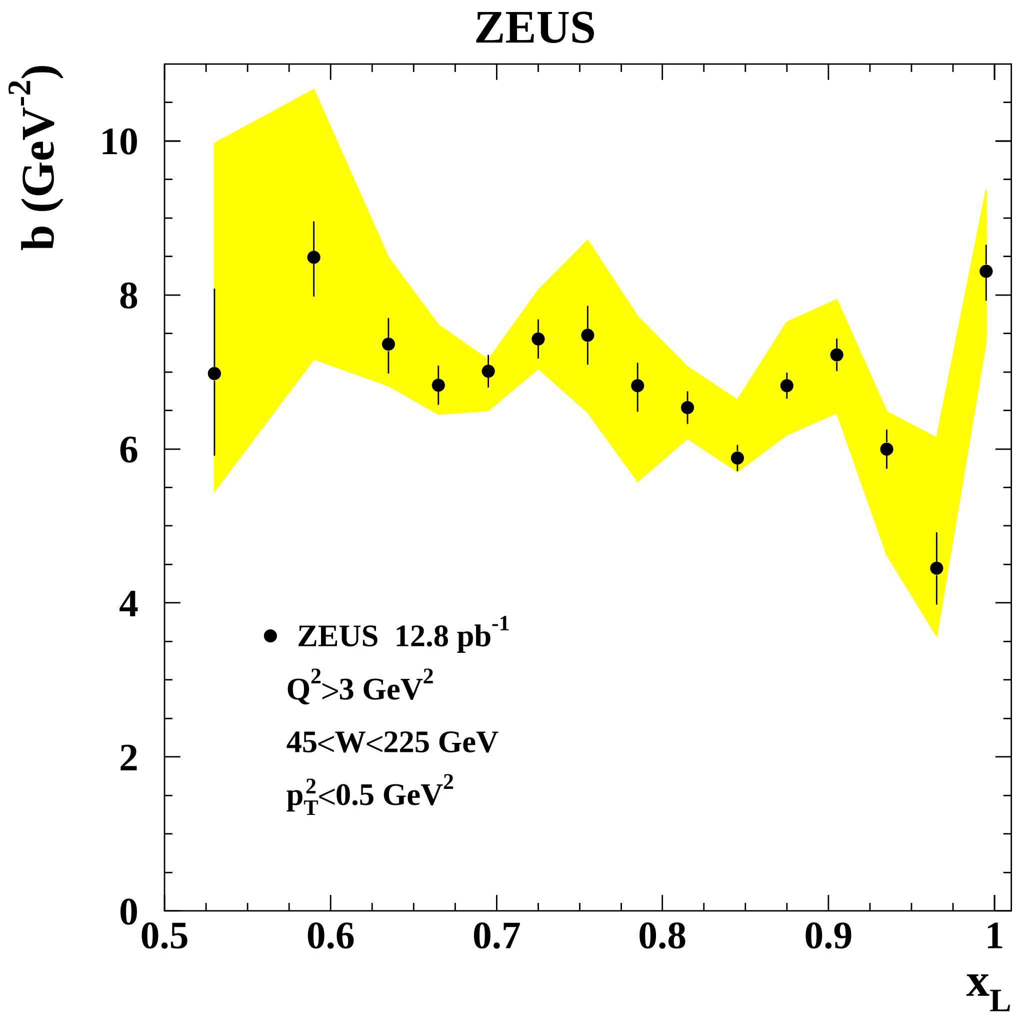

Figure 7: *The p_T^2-slope, b, of the cross section $d^2\sigma_{\rm LP}/dx_L dp_T^2$ as obtained by a fit to the data of a function $A \cdot e^{-b \cdot p_T^2}$ in bins of x_L, in the kinematic range indicated in the figure. The band represents the systematic uncertainty.*

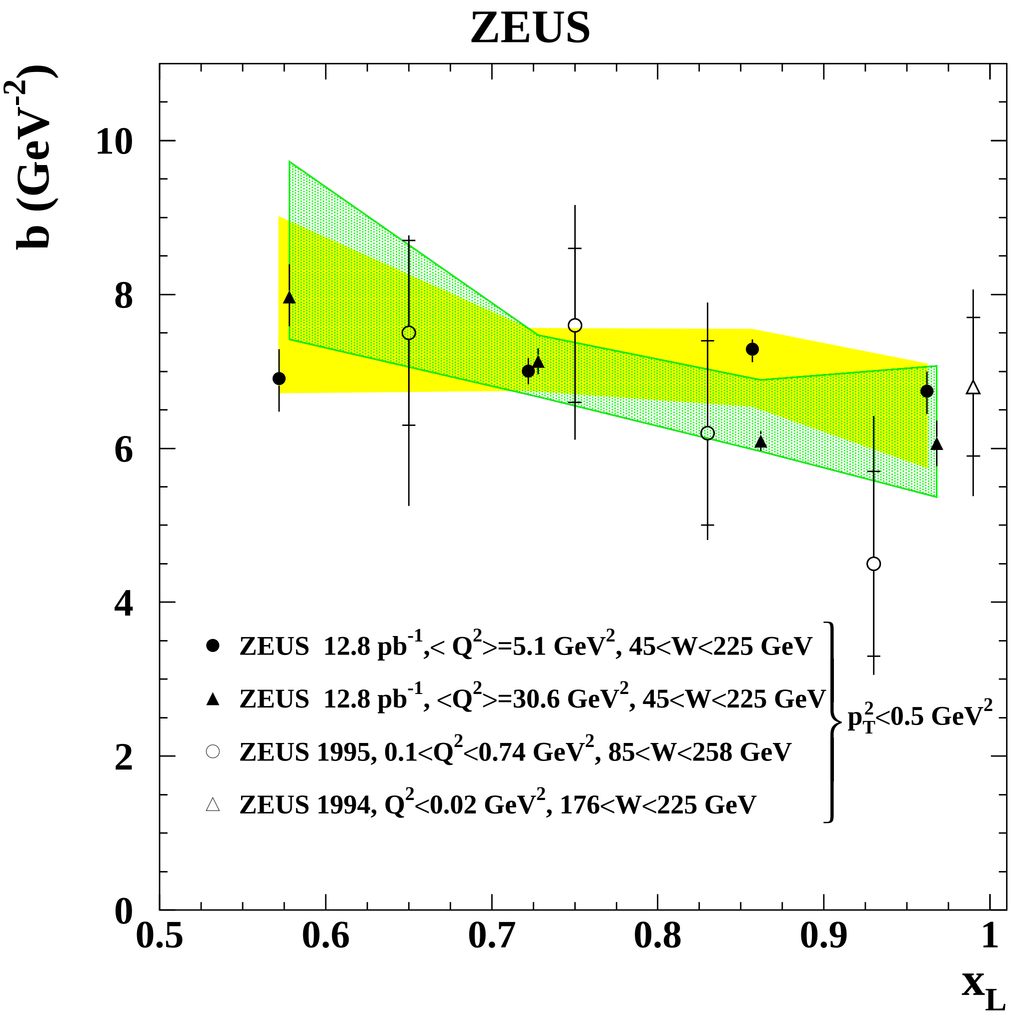

Figure 8: *The p_T^2-slope, b, of the cross section $d^2\sigma_{\rm LP}/dx_L dp_T^2$ in bins of x_L in different kinematic ranges as indicated in the figure. The bands represent the systematic uncertainty. For the ZEUS 1995 data [7] and the ZEUS 1994 data [16], the inner vertical bars show the statistical uncertainties, while the outer bars the statistical and systematic uncertainties added in quadrature.*

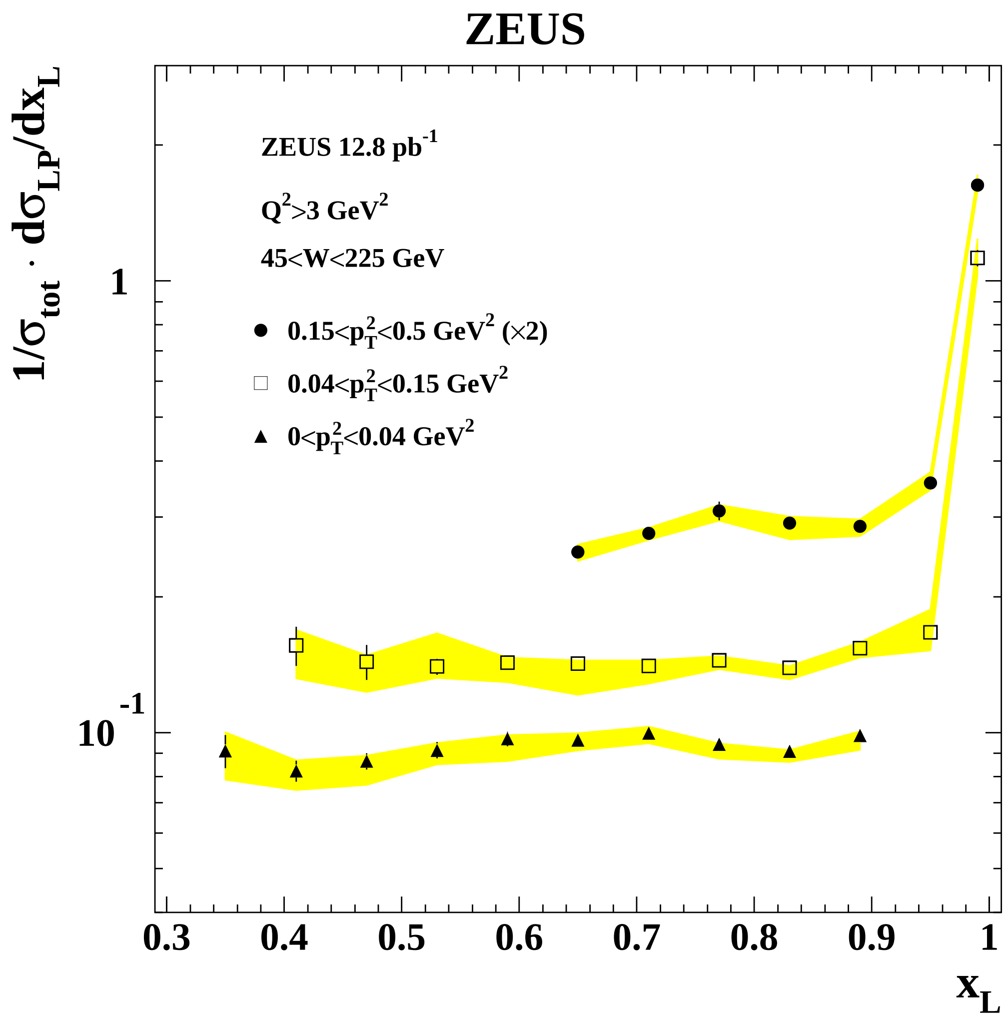

Figure 9: *The leading-proton production rate $1/\sigma_{\rm tot} \cdot \sigma_{\rm LP}/dx_L$ as a function of x_L in three p_T^2 ranges as indicated in the figure. The measurements in the higher p_T^2 range are multiplied by a factor two for visibility. Other details as in Fig. 7.*

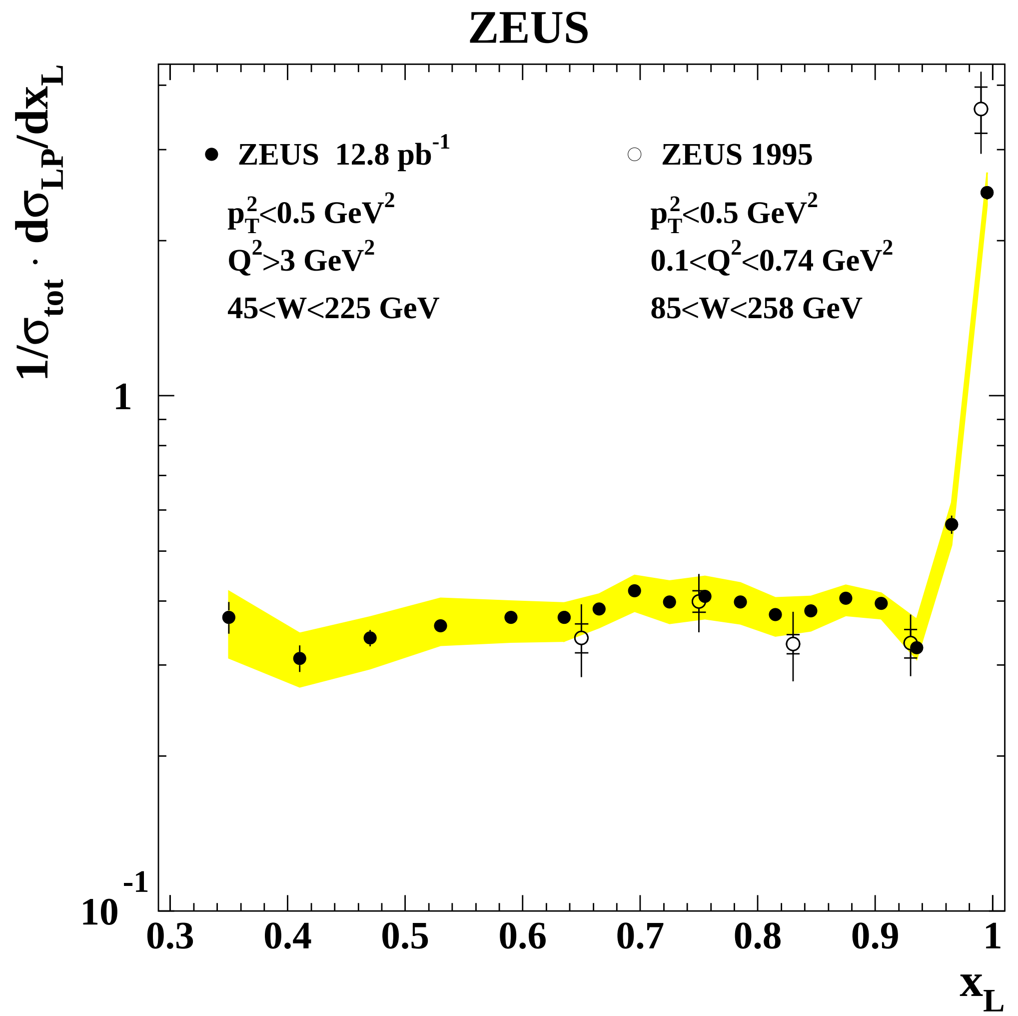

Figure 10: *The leading-proton production rate $1/\sigma_{\rm tot} \cdot d\sigma_{\rm LP}/dx_L$ for two ranges of Q^2 as indicated in the figure. Other details as in Fig. 8.*

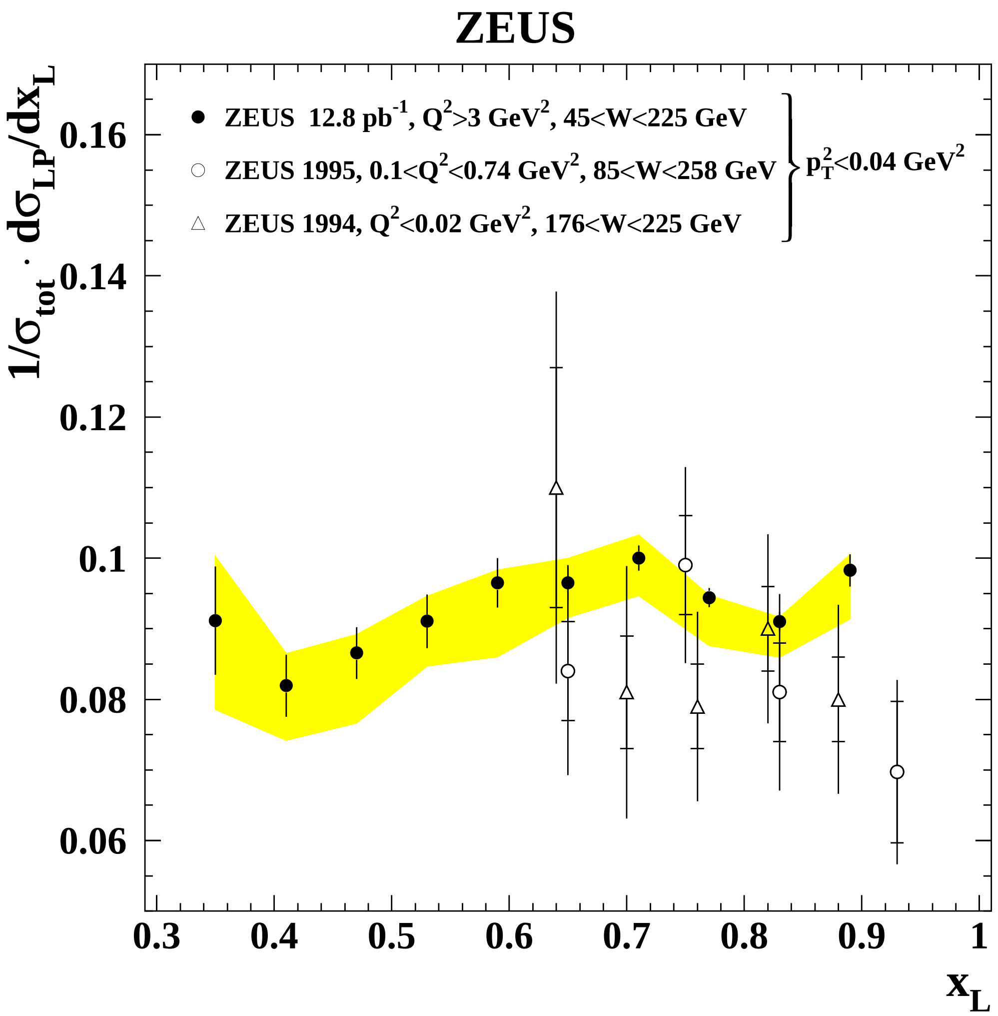

Figure 11: *The leading-proton production rate* $1/\sigma_{\rm tot} \cdot d\sigma_{\rm LP}/dx_L$ *for* $p_T^2 < 0.04$ *GeV*^{2} *in the kinematic ranges indicated in the figure. Other details as in Fig. 8.*

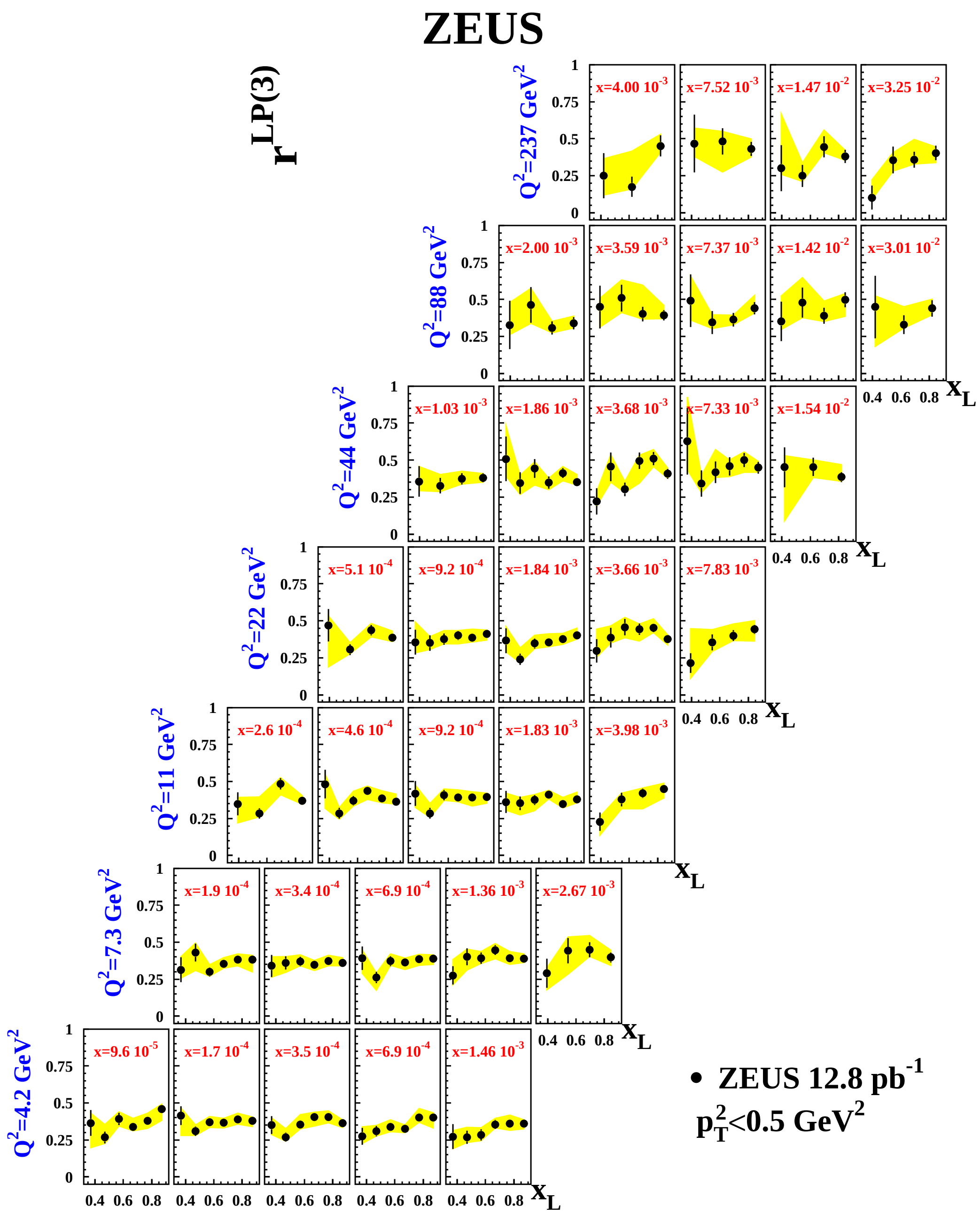

Figure 12: *The leading-proton production rate $r^{\mathrm{LP}(3)}$ as a function of x_L in bins of x and Q^2, for $p_T^2 < 0.5$ GeV^2. Other details as in Fig. 7*

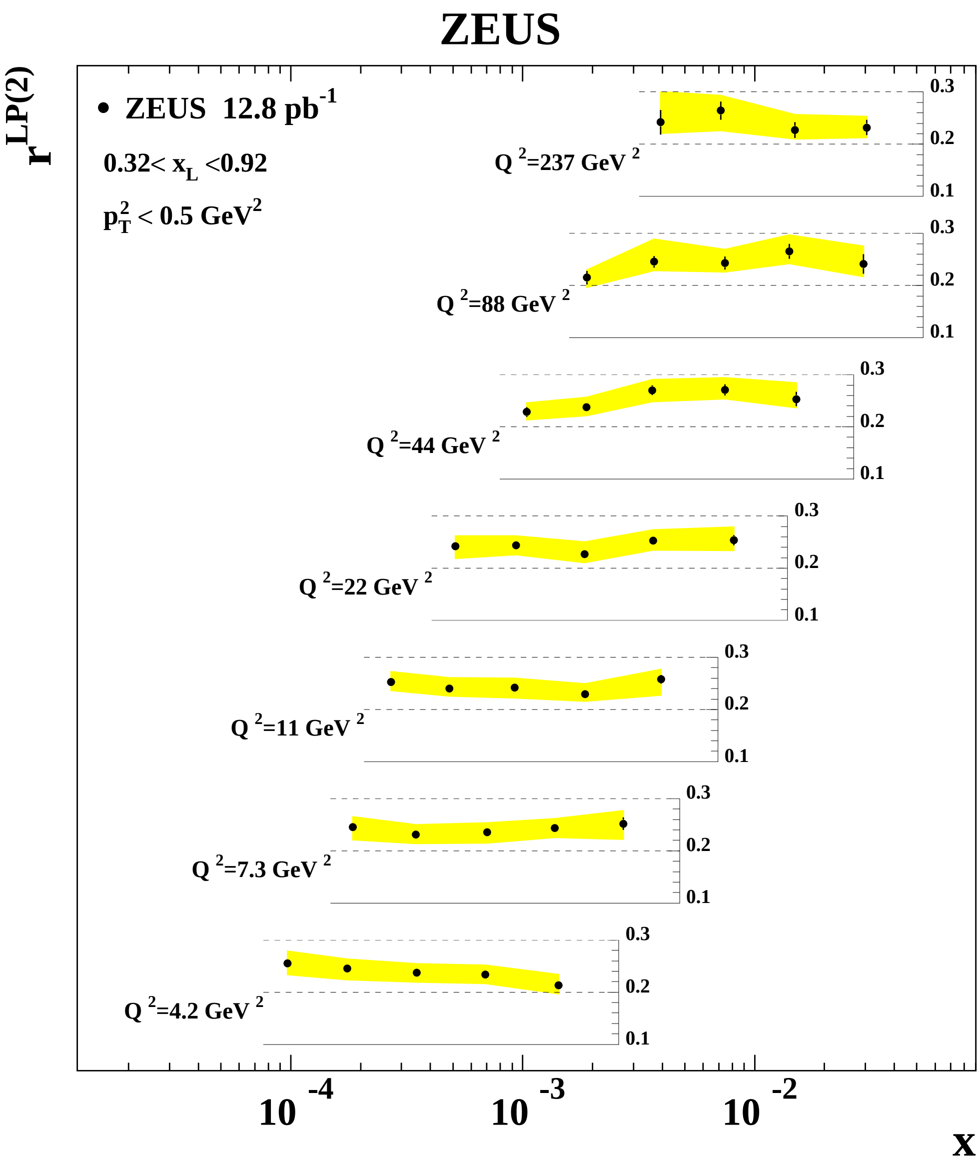

Figure 13: *The leading-proton production rate $r^{\mathrm{LP(2)}}$ as a function of x in bins Q^2, in the kinematic range indicated in the figure. The band represents the correlated systematic uncertainty.*

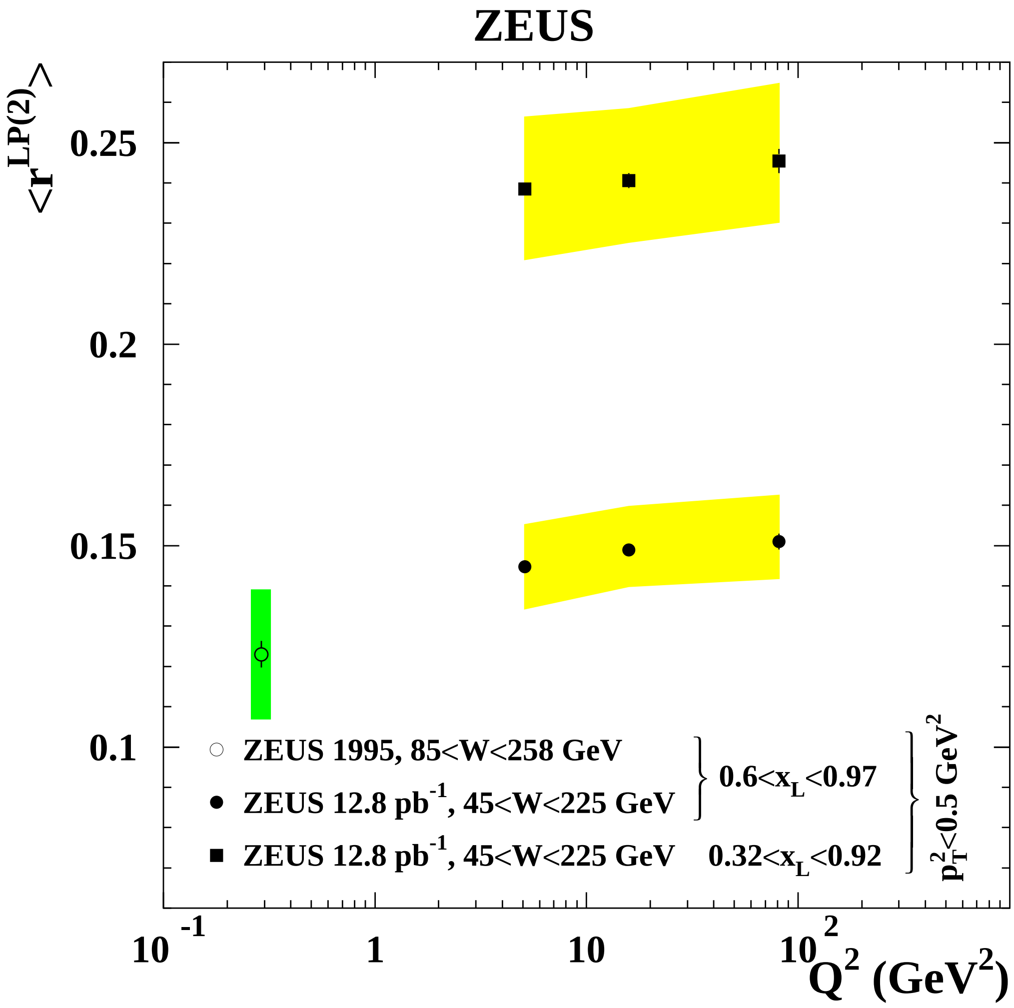

Figure 14: *The leading-proton production rate $\langle r^{\mathrm{LP}(2)} \rangle$, averaged over x, as a function of Q^2 in two different ranges of x_L, in the kinematic range indicated in the figure. The band represents the correlated systematic uncertainty. Other details as in Fig. 8.*

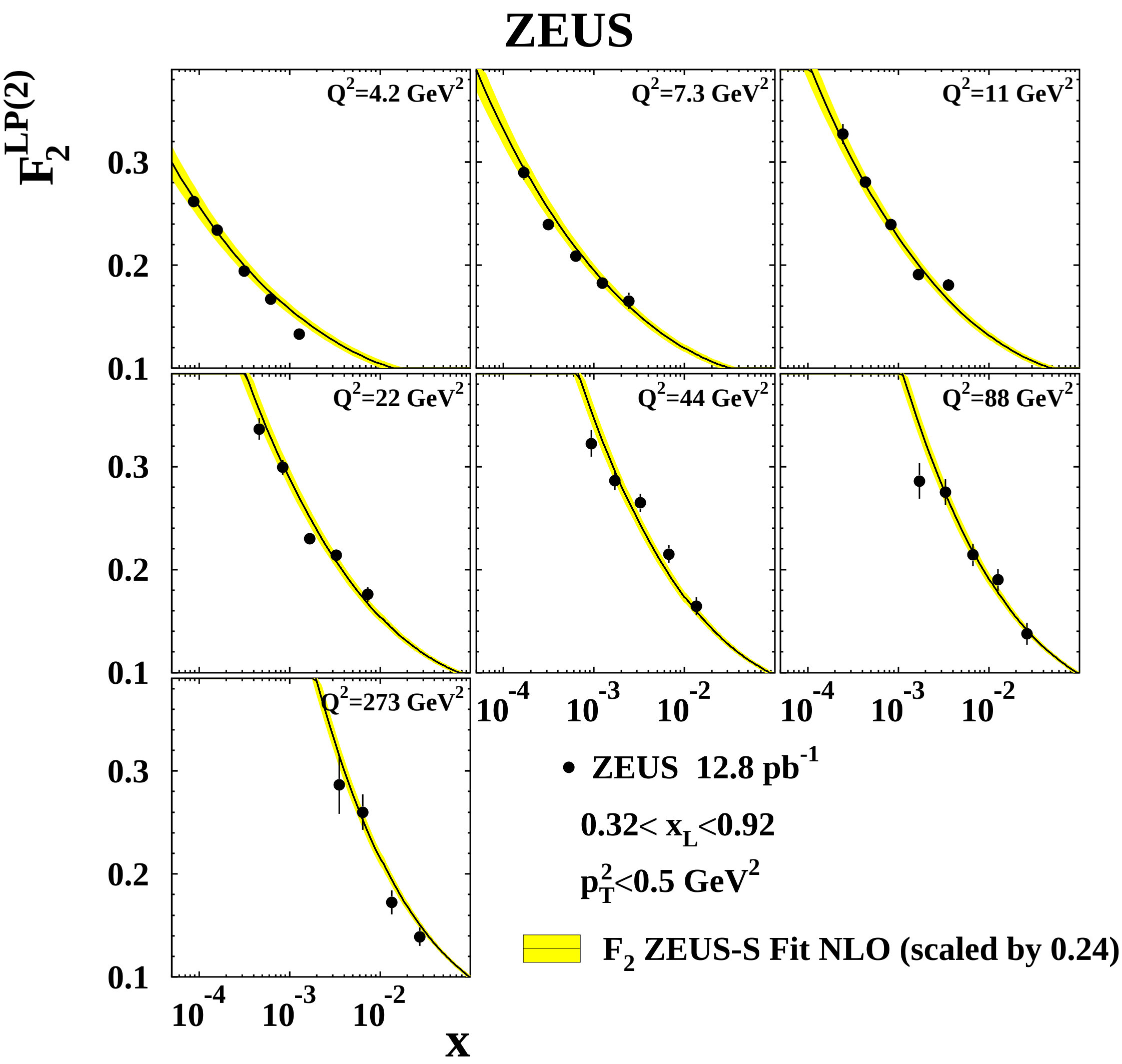

Figure 15: *The leading-proton structure function $F^{\mathrm{LP}(2)}$ as a function of x in bins of Q^2, in the kinematic range indicated in the figure. For the sake of clarity, only the statistical uncertainties are shown. The systematic uncertainties are listed in Table 12. The lines show the F_2 parametrization scaled by 0.24, the approximate average value of $r^{\mathrm{LP}(2)}$. The bands show the one-standard deviation limits of the F_2 parametrization.*

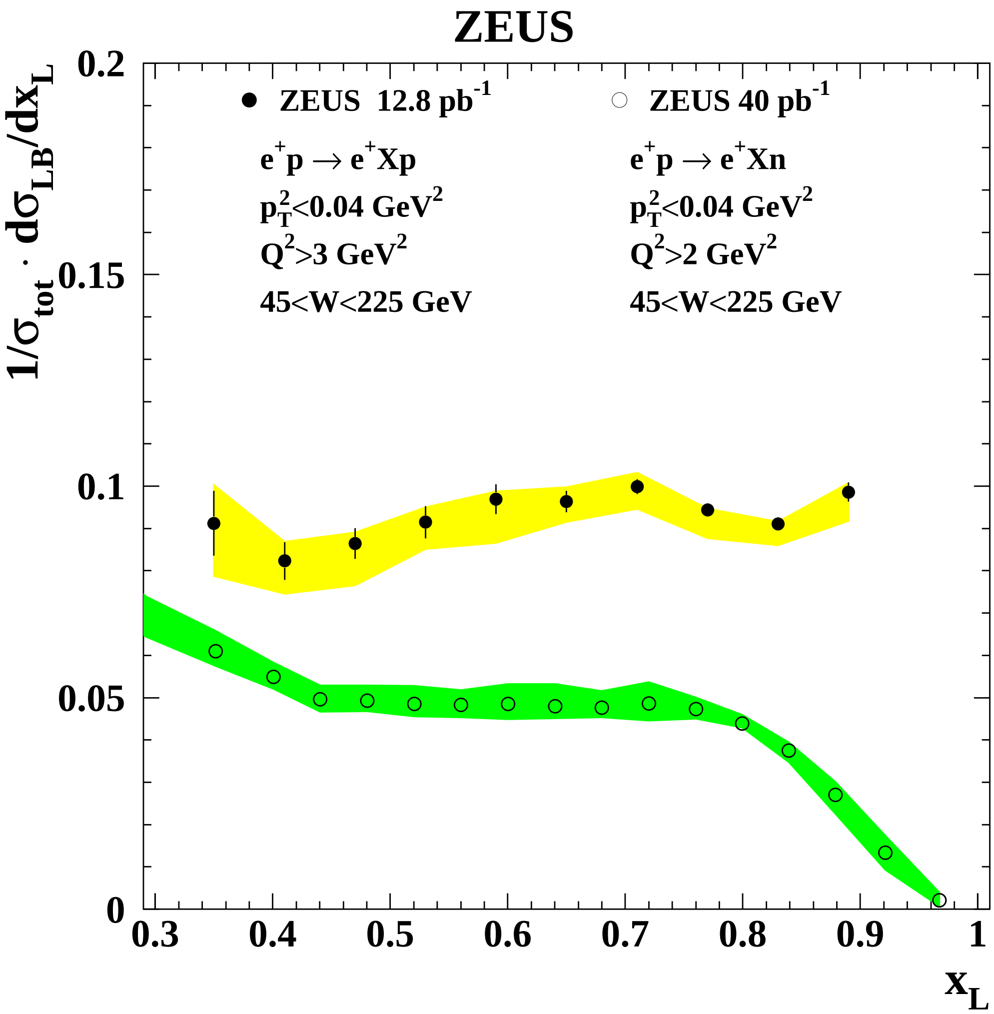

Figure 16: *The rate $1/\sigma_{\rm tot} \cdot d\sigma_{\rm LB}/dx_L$ for leading-proton (dots) and leading-neutron production (circles). The bands show the systematic uncertainties.*

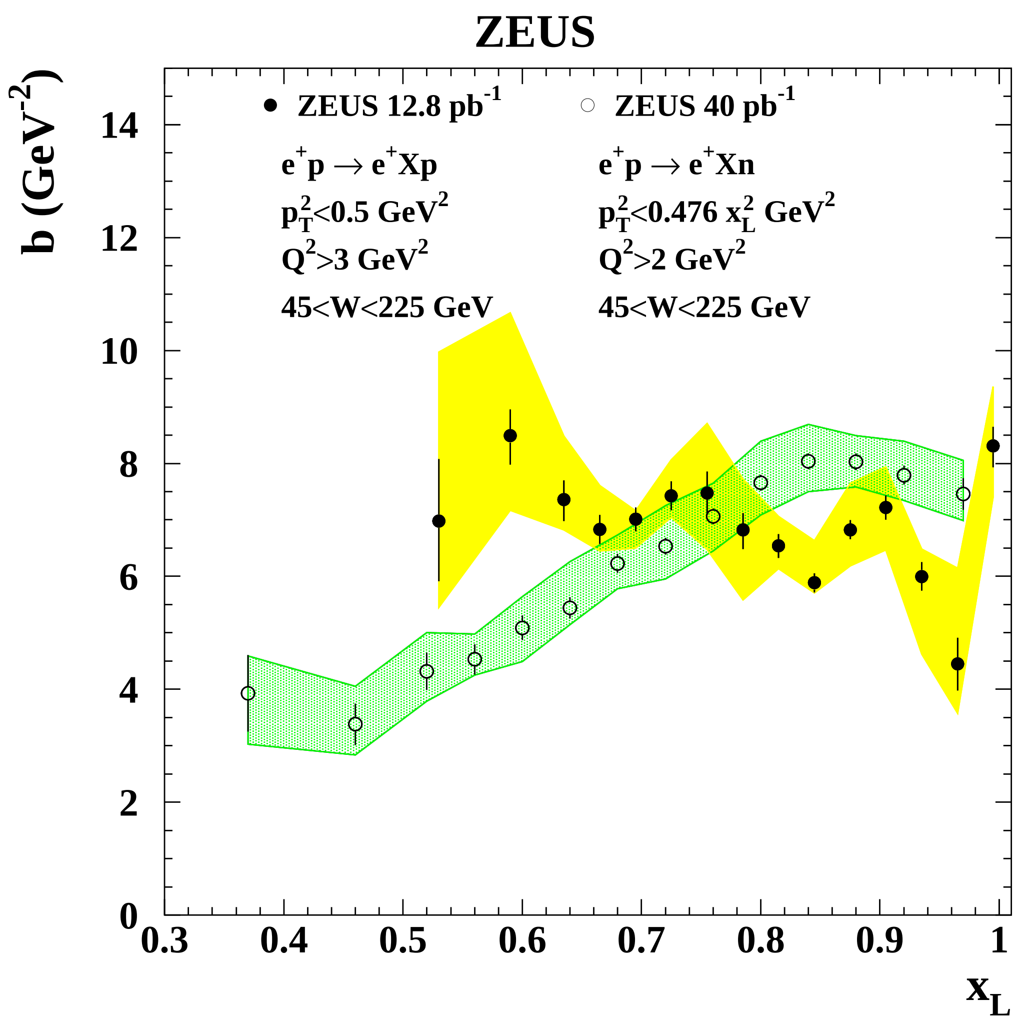

Figure 17: *The p_T^2-slope, b, as a function of x_L for leading-proton (dots) and leading-neutron (circles) production. The bands show the systematic uncertainties.*

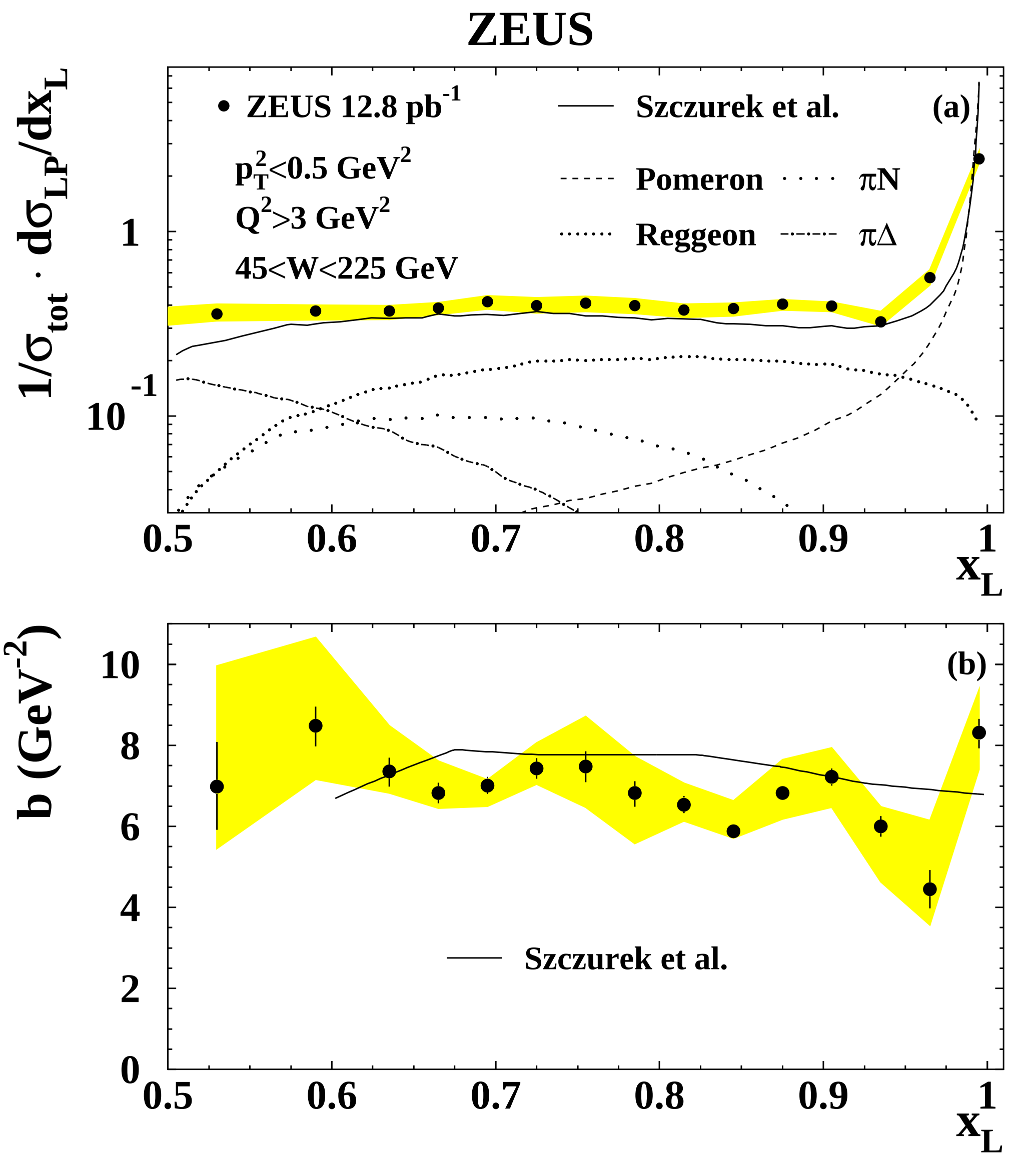

Figure 18: *A Regge-based model [13] compared to (a) the measured leading-proton production rate, $1/\sigma_{\rm tot} \cdot d\sigma_{\rm LP}/dx_L$, and (b) p_T^2-slope, b. The bands show the systematic uncertainties.*

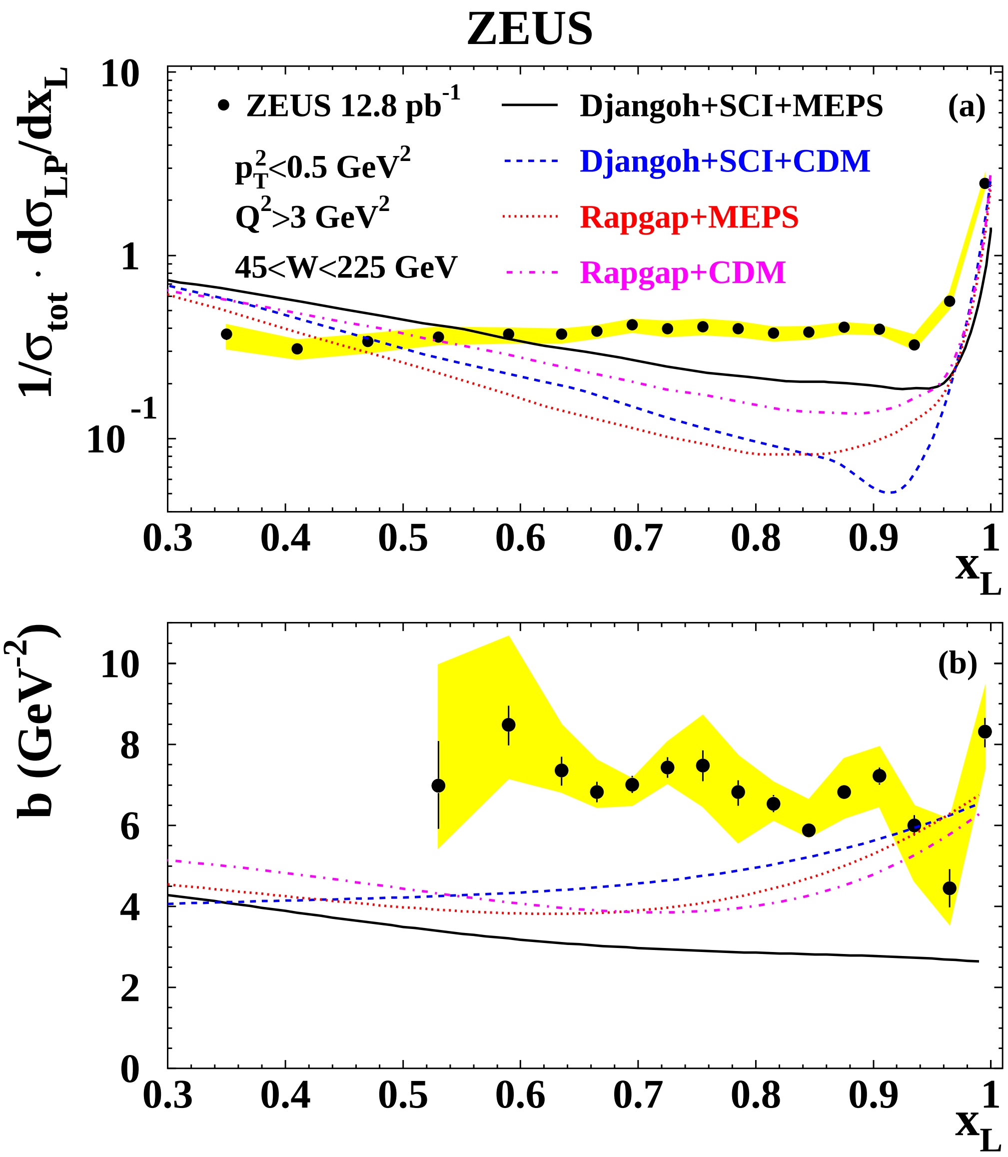

Figure 19: *Expectations of various Monte Carlo models of DIS, as described in the figure, compared to (a) the leading-proton production rate,* $1/\sigma_{\rm tot} \cdot d\sigma_{\rm LP}/dx_L$*, and (b)* p_T^2*-slope, b. The bands show the systematic uncertainties.*